Pollen tube-triggered accumulation of NORTIA at the filiform apparatus facilitates fertilization in *Arabidopsis thaliana*

Jing Yuan[1,2*], Yan Ju[1,2*], Daniel S. Jones[4,5], Weiwei Zhang[2,3], Noel Lucca[1,2], Christopher J. Staiger[1,2,3], and Sharon A. Kessler[1,2,**]

[1]Department of Botany and Plant Pathology, Purdue University, West Lafayette, Indiana USA
[2]Purdue Center for Plant Biology, Purdue University, West Lafayette, Indiana USA
[3]Department of Biological Sciences, Purdue University, West Lafayette, Indiana USA
[4]Biology Department, The University of North Carolina at Chapel Hill, Chapel Hill, North Carolina USA (current address)
[5]Department of Microbiology and Plant Biology, University of Oklahoma, Norman, Oklahoma USA
*These authors contributed equally

** Corresponding author
Email: sakessler@purdue.edu

Abstract

During gamete delivery in *Arabidopsis thaliana*, intercellular communication between the attracted pollen tube and the receptive synergid cell leads to subcellular events in both cells culminating in the rupture of the tip-growing pollen tube and release of the sperm cells to achieve double fertilization. Live imaging of pollen tube reception revealed dynamic subcellular changes that occur in the female synergid cells. Pollen tube arrival triggers the trafficking of NORTIA (NTA) MLO protein from Golgi-associated compartments and the accumulation of endosomes at or near the synergid filiform apparatus, a membrane-rich region that acts as the site of communication between the pollen tube and synergids. Domain swaps and site-directed mutagenesis reveal that NTA's C-terminal cytoplasmic tail with its calmodulin-binding domain influences the subcellular localization and function of NTA in pollen tube reception and that

accumulation of NTA at the filiform apparatus is necessary and sufficient for MLO function in pollen tube reception.

Key words

MLO, pollination, gametophyte, synergid, pollen tube reception, calmodulin binding domain, pollen tube

Introduction

Intercellular communication is central to the proper development and maintenance of all multicellular organisms. During this communication, signals from one cell are perceived by receptors in another cell and translated into various subcellular responses. These responses include signal transduction cascades leading to transcription of other genes, calcium signaling, and trafficking of proteins to different organelles or regions of the cell. A well-studied example of signal-induced protein trafficking in plant development is the redistribution of the PIN polar auxin transporters to different sides of the cell during important developmental events such as embryo patterning, leaf initiation and lateral root initiation [1-3]. In plants, most intercellular communication occurs between cells that are genetically identical and connected by adjoining cell walls. One exception is pollination, in which pollen (the male gametophyte) is released from an anther, transported to a receptive stigma, and produces a tip-growing pollen tube that grows through the female tissues of the pistil and delivers the two sperm cells to the female gametophyte (also known as the embryo sac, Figure 1A). The pollen tube's journey through the pistil requires cell-to-cell interactions with the female that allows water and nutrient uptake and enables the detection of cues important for guidance toward the female gametes [4].

In the model plant *Arabidopsis thaliana*, complex signaling events ranging from pollen landing on the stigma to fusion of gametes occur over several hours. Most of our knowledge about the signaling pathways involved along the pollen tube's journey through the female is limited to the

56 final stages of pollination and involve a highly specialized pair of female gametophyte cells
57 known as synergids. During female gametophyte development, meiosis followed by three
58 rounds of mitosis produce the egg cell and central cell along with 2 synergid cells flanking the
59 egg cell and 3 antipodal cells on the chalazal end of the embryo sac [5] (Figure 1A). The
60 synergid cells are accessory cells that control the behavior of the pollen tube during the final
61 stages of pollination. Before pollen tube arrival, they secrete cysteine-rich LURE peptides that
62 act as short-range pollen tube attractants that are recognized by receptor-like kinases in the tip
63 of the pollen tube to regulate the direction of pollen tube growth and guide the pollen tube to the
64 micropyle of the ovule [6-8]. After pollen tube arrival, the synergids communicate with the pollen
65 tube to induce changes that result in pollen tube rupture and delivery of the sperm cells [4, 9].
66 Thus, synergids are critical for ensuring that double fertilization can occur to produce seeds.
67
68 In Arabidopsis, live imaging has been used to examine the behavior of both the pollen tube and
69 the synergids during the process of pollen tube reception. A pollen tube follows the gradient of
70 LURE attractants, enters the micropyle of the ovule, and pauses its growth for 30 min to 1 h just
71 outside the receptive synergid [10-12]. During this pause in pollen tube growth, communication
72 occurs between the pollen tube and the synergids leading to subcellular changes and ultimately
73 the death of both the pollen tube and the receptive synergid. Cytoplasmic calcium oscillations
74 occur in both the tip of the pollen tube and in the 2 synergid cells during this communication
75 phase. Cytoplasmic calcium levels continue to increase in both cell types until the pollen tube
76 starts to grow again and bursts to release the sperm cells, a catastrophic event for both the
77 pollen tube and the receptive synergid, which also degenerates [10-12]. Mutations in genes that
78 regulate communication between the synergids and pollen tube during pollen tube reception
79 result in a pollen tube overgrowth phenotype in which the pollen tubes are attracted normally to
80 the ovules, but do not get the signal to burst and release the sperm cells. Presumably, synergid-
81 induced changes in the cell wall of the pollen tube tip do not occur in these mutants, therefore

82 the pollen tube continues to grow and coil inside the embryo sac. Synergid-expressed genes
83 that participate in pollen tube reception include the FERONIA (FER) receptor-like kinase, the
84 GPI-anchored protein LORELEI (LRE), and the Mildew Resistance Locus-O (MLO) protein
85 NORTIA (NTA, also known as AtMLO7) [12-17]. Mutations in all of these genes lead to the
86 pollen tube overgrowth phenotype due to disruption of the pollen tube-synergid communication
87 pathway.
88
89 FER and LRE are necessary for the calcium oscillations that occur in synergids in response to
90 pollen tube arrival [12]. In contrast, *nta-1* mutants have $[Ca^{2+}]_{cyto}$ oscillations at lower amplitudes,
91 indicating that NTA may participate in modulating Ca^{2+} fluxes in the synergids during
92 communication with the pollen tube and likely act downstream of FER and LRE [12]. Like all
93 members of the MLO gene family, NTA has seven membrane-spanning domains and a
94 predicted calmodulin-binding domain (CaMBD) in its C-terminal intracellular tail [18, 19].
95 Calmodulin (CaM) is a small protein that binds Ca^{2+} and is involved in signal transduction for
96 many cellular processes [20]. We previously showed that the C-terminal domain of NTA could
97 confer pollen tube reception function to the related MLO8 protein [21], but the significance of the
98 CaMBD in pollen tube reception remains an open question.
99
100 The subcellular localization of important pollen tube reception proteins is not always predictive
101 of their function in communicating with the pollen tube. As expected for early response proteins,
102 both FER and LRE are expressed in synergid cells where they localize in or near a specialized
103 region called the filiform apparatus, a membrane rich area located at the micropyle end of the
104 synergids [14-17, 22-24]. The filiform apparatus is thought to be important for the secretion of
105 attractant peptides and is the first site of interaction between the pollen tube and synergid cell
106 prior to pollen tube reception [25-27]. In contrast, before pollen tube arrival, NTA is localized to a
107 Golgi-associated compartment within the synergid cell and absent from the filiform apparatus

108 [21]. At the end of pollen tube reception, NTA protein is only detected at the filiform apparatus,
109 indicating that this protein changes its subcellular localization during pollen tube reception [13].
110 This suggests that pollen tube-triggered regulation of the synergid secretory system may be a
111 crucial subcellular response to pollen tube arrival and that NTA function may be related to its
112 subcellular distribution; however, the precise timing and significance of NTA's redistribution
113 remain unclear.
114
115 Here, we use a live-imaging system to further characterize synergid cellular dynamics during
116 pollen tube reception and to determine the timing and significance of the polar redistribution of
117 NTA to the filiform apparatus. To investigate the link between Ca^{2+} and MLO function in pollen
118 tube reception, we assayed the influence of the CaMBD on NTA's function and subcellular
119 distribution through C-terminal truncations and a point mutation disrupting the CaMBD. We
120 show that the polar redistribution of NTA is triggered by the approach of a pollen tube and is
121 facilitated by the CaMBD. While most subcellular compartments remain distributed throughout
122 the synergid cells during pollen tube reception, recycling endosomes respond to pollen tube
123 arrival by accumulating towards the filiform apparatus. Manipulation of NTA subcellular
124 localization with domain swaps and a Golgi retention signal revealed that filiform apparatus
125 localization is necessary and sufficient for MLO function in pollen tube reception.
126
127 **Results**
128 **NTA dynamically accumulates at the filiform apparatus during pollen tube reception**
129 Pollen tube reception requires synergid cells to recognize the approaching pollen tube and to
130 send signals back to the pollen tube that result in release of the sperm cells at the correct time
131 and place so that double fertilization can be completed. Based on static images, we previously
132 reported that NTA-GFP fusion protein localizes to a Golgi-associated compartment in synergids
133 prior to pollen tube attraction [21]. When imaged after pollen tube reception, NTA-GFP is

concentrated at the micropylar end of the synergid (in or near the filiform apparatus) [13]. NTA-GFP does not accumulate at the filiform apparatus in *fer* ovules with pollen tube overgrowth, suggesting that FER-mediated signaling during pollen tube reception triggers NTA-GFP redistribution that in turn contributes to the interaction of the synergid with the pollen tube [13]. An alternative hypothesis is that pollen tube rupture triggers NTA-GFP redistribution and is a symptom of pollen tube reception rather than an important contributor to the signaling pathway. To distinguish between these two possibilities, we used a semi-*in vivo* pollination system combined with time-lapse spinning disk confocal microscopy to determine the timing of NTA-GFP redistribution during the pollen tube reception process. In the semi-*in vivo* system, pollen tubes grow out of a cut style and are attracted to ovules arranged on pollen germination media [28]. This system has previously been used to quantify and track pollen tube attraction to ovules and to image $[Ca^{2+}]_{cyto}$ reporters during pollen tube reception [10, 12, 29-32]. To follow subcellular changes in NTA-GFP protein localization before, during, and after pollen tube arrival, we used pollen from plants expressing the pollen-specific *AUTOINHIBITED* Ca^{2+}-*ATPase9*$_{pro}$*::DsRed* (*ACA9*$_{pro}$*::DsRed*) reporter and ovules expressing *NTA*$_{pro}$*::NTA-GFP* in the semi-*in vivo* system. Approximately 4 h after pollination, pollen tubes emerged from the style onto the media and were attracted to ovules (Figure 1B). Fluorescence images in both channels were collected every 5 min from when a pollen tube approached an ovule until after the pollen tube ruptured inside the ovule. In ~83% (n=93) of the ovules that attracted a pollen tube and successfully burst to deliver the sperm cells, NTA-GFP accumulated at the filiform apparatus of the synergids (Figures 1C-E). The rest of the ovules (~17%) attracted pollen tubes that stopped growing in the micropyle and did not rupture. In these ovules, NTA-GFP did not accumulate at the filiform apparatus. To exclude the possibility that prolonged imaging causes stress in synergids which leads to filiform apparatus accumulation of NTA-GFP, we analyzed neighboring ovules that did not attract pollen tubes but were imaged together with ovules that attracted pollen tubes. NTA-GFP did not accumulate at the filiform apparatus in these ovules (n=103)

160 (Figure 1F). Likewise, ovules that were incubated on pollen germination media without a
161 pollinated pistil (n=133, Figures 1F and S1) and imaged over the same time frame did not
162 accumulate NTA-GFP at the filiform apparatus. These data indicate that pollen tube arrival is
163 necessary for NTA-GFP accumulation at the filiform apparatus rather than being retained in the
164 Golgi, and that this accumulation is not an artifact of the semi- *in vivo* imaging system. (Figure
165 1F).
166
167 Our semi-*in vivo* system also allowed us to determine the timing of NTA-GFP accumulation at
168 the filiform apparatus in relation to the position of the pollen tube as it approached the
169 synergids. We defined the 0 min timepoint as the time where the pollen tube just reached the
170 micropylar opening of the ovule (Figure 1C, ovules with yellow stars, Movies S1 and S2). In all
171 cases, the shift of NTA-GFP signal from the Golgi to the filiform apparatus also started from this
172 time point. During the following 30–50 min, pollen tubes grew through the micropyle region of
173 ovule and arrived at the filiform apparatus of the receptive synergid cell. During this timeframe,
174 three quarters to half of the NTA-GFP signal moved to the micropylar end of synergid cells,
175 indicating that the approach of the pollen tube triggers NTA-GFP accumulation at the filiform
176 apparatus. As reported in [12] and [10], the arriving pollen tubes paused their growth outside the
177 filiform apparatus for 30–50 min, presumably for cell-to-cell communication. During this period,
178 the NTA-GFP signal continued to shift toward the filiform apparatus. At 70–80 min after pollen
179 tube arrival at the micropyle, NTA-GFP signal was only detected at the filiform apparatus and
180 pollen tubes resumed growth and ruptured to release the sperm cells (Figures 1C, D and
181 Movies S1 and S2). Even though only one of the synergids receives the pollen tube, NTA-GFP
182 accumulated at the filiform apparatus in both synergid cells in response to pollen tube arrival,
183 similar to the activation of $[Ca^{2+}]_{cyto}$ oscillations in both synergids during pollen tube reception
184 reported in [12].
185

186 **Golgi do not concentrate at the filiform apparatus during pollen tube reception**

187 We previously determined that NTA is sequestered in a Golgi-associated compartment in
188 synergid cells that have not attracted a pollen tube [21]. Our live-imaging data suggest that
189 NTA-GFP is selectively moved out of the Golgi and transported to the filiform apparatus in
190 response to pollen tube arrival. However, it is possible that the observed NTA-GFP
191 accumulation at the filiform apparatus is a result of massive reorganization of subcellular
192 compartments. To distinguish between these possibilities, we investigated the behavior of the
193 Golgi in synergid cells during pollen tube reception. We used the semi-*in vivo* imaging system
194 described above with a synergid-expressed Golgi marker (Man49-mCherry) co-expressed with
195 NTA-GFP [33]. In all replicates, the Golgi marker was distributed throughout the synergids,
196 excluded from the filiform apparatus, and co-localized with NTA-GFP as reported previously
197 (Figure 2A, n=93). When a pollen tube approached the synergids, NTA-GFP accumulated at the
198 filiform apparatus of the synergids as observed previously (Figure 1), but the Golgi-mCherry
199 marker remained consistently distributed throughout the synergid cells and did not concentrate
200 near the filiform apparatus (Figure 2B). In order to examine the behavior of the Golgi during later
201 stages of pollen tube reception, we used the synergid-expressed Golgi marker line
202 (*LRE*$_{pro}$*::Man49-mCherry*) and pollen that was expressing GFP (*Lat52*$_{pro}$*::GFP*). In all cases, the
203 Golgi marker remained randomly distributed throughout the synergid cells, even after pollen
204 tube rupture (Figures 2C-D, Movies S3 and S4, n=106). These results indicate that the
205 accumulation of NTA-GFP at the filiform apparatus during pollen tube reception is not linked to
206 mass redistribution of Golgi.

207

208 **Endosomes accumulate at the filiform apparatus during pollen tube reception**

209 A signal from the arriving pollen tube seems to trigger the movement of NTA-GFP out of the
210 Golgi-associated compartments. It is possible that pollen tube arrival triggers other changes to
211 synergid subcellular organization. We previously reported the localization of synergid-expressed

212 markers for the ER, peroxisome, endosome and the trans-Golgi Network (TGN) in unfertilized
213 ovules *in vivo* using confocal laser scanning microscopy [33]. Before pollen tube arrival, SP-
214 mCherry-HDEL (an ER-associated marker), mCherry-SKL (a peroxisome-associated marker),
215 and mCherry-RabA1g (a recycling endosome-associated marker) were all distributed evenly
216 throughout synergid cells (Figures S2-S4 and 3A; [33]. The TGN-associated marker SYP61
217 exhibited two types of distribution patterns before pollen tube arrival: in type 1 synergids, the
218 marker accumulated near the filiform apparatus, whereas type 2 synergids displayed a punctate
219 distribution pattern throughout the cells (Figure S3; [33]. During pollen tube reception, no
220 change was seen in the TGN marker distribution in either type of synergids (Figure S3, Movies
221 S5 and S6). Likewise, the ER and peroxisome markers maintained a diffuse distribution
222 throughout the synergids and did not accumulate at the filiform apparatus (Figures S2 and S4,
223 Movies S7-10). In contrast, we detected a more dynamic behavior of the endosome marker
224 during pollen tube reception. Endosomes are membrane-bound compartments that are involved
225 in the endocytic membrane transport pathway from the plasma membrane to the vacuole.
226 Endosomes also transport molecules from the Golgi and either continue to the vacuole or
227 recycle back to the Golgi [34]. We previously reported that mCherry-RabA1g is distributed
228 throughout synergid cells and had some overlap with NTA-GFP in synergids of unpollinated
229 ovules [33]. Using the semi-*in vivo* system, we confirmed that before pollen tube arrival,
230 mCherry-RabA1g distributed throughout synergid cells (Figure 3A). Interestingly, as pollen
231 tubes approached, the endosome marker started to accumulate at the filiform apparatus of the
232 synergid cells (Figures 3A and B). By the time pollen tube reception was completed, most of the
233 endosome signal was concentrated at or near the filiform apparatus (Figures 3B-F and S5,
234 Movies S11 and S12). These results indicate that the RabA1g endosome compartments have a
235 distinct response to pollen tube arrival and may play a role in facilitating the intercellular
236 signaling pathway that occurs between the synergids and the pollen tube.
237

238

239 **Pollen tube-independent targeting of NTA to the filiform apparatus is not toxic to the**
240 **synergids**

241 The selective targeting of NTA-GFP from the Golgi to the filiform apparatus during pollen tube
242 arrival (Figures 1 and 2) suggests that NTA trafficking to the pollen tube/synergid interface is
243 important for the intercellular communication process that occurs between the pollen tube and
244 synergids. In *nta-1* mutants, around 30% of ovules display pollen tube overgrowth and fail to
245 complete double fertilization, but the other 70% are fertilized normally [13]. This indicates that
246 NTA is not absolutely required for pollen tube reception, but may function as a modifier of the
247 signaling pathway. Since FER signaling in the synergids leads to cell death as pollen tube
248 reception is completed [17, 23, 24], NTA trafficking to the filiform apparatus could be a
249 mechanism to regulate this death and would thus require sequestration of "toxic" NTA in the
250 Golgi before pollen tube arrival. To test this hypothesis, we took advantage of sequence
251 variation leading to differential subcellular localization of MLO proteins to manipulate the
252 subcellular localization of NTA. When expressed in synergids, other proteins from the
253 Arabidopsis MLO family have different subcellular localization patterns, indicating that specific
254 sequences within the MLOs direct them to different parts of the secretory system [35]. MLO1-
255 GFP localizes at the filiform apparatus when it is ectopically expressed under control of the
256 synergid-specific *MYB98* promoter and cannot complement the *nta-1* pollen tube reception
257 phenotype [21], and Figure 4C and 4G). Domain swaps between different regions of NTA and
258 MLO1 revealed that the C-terminal cytoplasmic tail including the CaMBD of MLO1 (NTA-
259 MLO1^{CTerm}, see diagram in Figure 4D) was sufficient to direct the fusion protein to the filiform
260 apparatus of the synergids, in a pattern very similar to MLO1-GFP (Figure 4C). Quantification of
261 the GFP signal along the length of the synergids from the chalazal end to the filiform apparatus
262 in the NTA-GFP, NTA-MLO1^{Cterm}-GFP, and MLO1-GFP confirmed that the MLO1 tail was
263 sufficient to cause NTA protein accumulation at the filiform apparatus (Figure 4A, 4C and 4D). In

264 MLO1-GFP and NTA-MLO1^{Cterm}-GFP ovules, the majority of GFP signal was detected in the 20-
265 40% of the micropylar pole of synergids and most of the signal overlapped with the diffuse FM4-
266 64 staining at the filiform apparatus (Figure 4F). In contrast, wild-type NTA-GFP is excluded
267 from the filiform apparatus (Figure 4A and [21].
268
269 The successful manipulation of NTA subcellular localization provided a tool for determining the
270 functional relevance of NTA redistribution. We transformed the NTA-MLO1^{CTerm}-GFP construct
271 into *nta-1* plants and used the percentage of unfertilized ovules as a measurement for the ability
272 of the fusion construct to complement the *nta-1* phenotype of unfertilized ovules caused by
273 pollen tube overgrowth [13]. Synergid-expression of NTA-MLO1^{CTerm}-GFP rescued the *nta-1*
274 pollen tube reception phenotype (Figure 4G), indicating that 1) the MLO1^{CTerm} domain is
275 functionally equivalent to the NTA^{CTerm} domain when the protein is localized at the filiform
276 apparatus and 2) premature targeting of NTA to the filiform apparatus is not toxic to synergid
277 cells.
278
279 **Polar accumulation of NTA at the filiform apparatus is necessary for pollen tube**
280 **reception**
281 Early targeting of NTA-MLO1^{CTerm}-GFP to the filiform apparatus was sufficient to complement
282 the *nta-1* pollen tube reception phenotype, but did not give an indication of whether filiform
283 apparatus targeting is necessary for NTA function. Since NTA accumulation is triggered by the
284 arrival of a growing pollen tube, drugs that block membrane protein trafficking are not
285 appropriate to inhibit NTA accumulation at the filiform apparatus because they would also inhibit
286 pollen tube growth. Therefore, we used a genetic approach to inhibit NTA trafficking to the
287 filiform apparatus by adding a Golgi retention signal (RNIKCD) to the C-terminus of our MLO-
288 GFP variants. This Golgi retention signal has been reported to cause Golgi-retention when
289 added to proteins that would normally be targeted to the trans-Golgi network and tonoplast [36].

290 To test if RNIKCD works on MLO proteins, we added RNIKCD to the C-terminus of MLO1
291 (MLO1-RNIKCD) and NTA (NTA-RNIKCD) and co-infiltrated tobacco leaves with these
292 constructs and the Golgi-mCherry marker (*35S::Man49-mCherry*). Both NTA and NTA-RNIKCD
293 co-localize with Golgi-mCherry marker in tobacco leaves (Figure S7A), as was previously
294 reported for NTA-GFP [21]. However, in contrast to MLO1-GFP which accumulates at the
295 plasma membrane and not in the Golgi, most of MLO1-RNIKCD was retained in the Golgi
296 (Figure S7A). We next added RNIKCD to $MYB98_{pro}$-driven NTA and NTA-$MLO1^{CTerm}$ (NTA-
297 RNIKCD and NTA-$MLO1^{CTerm}$-RNIKCD) and transformed the constructs into *nta-1* and Golgi-
298 mCherry plants for functional and subcellular localization studies, respectively. In synergids of
299 emasculated ovules, both NTA-RNIKCD and NTA-$MLO1^{CTerm}$-RNIKCD fusion proteins co-
300 localized with the Golgi marker (Figure 4B, 4E and S7B), indicating that MLO fusion proteins
301 were mostly retained in the Golgi. Synergid-expressed NTA-RNIKCD and NTA-$MLO1^{CTerm}$-
302 RNIKCD could only partially rescue the *nta-1* pollen tube reception phenotype (Figure 4G),
303 indicating that filiform apparatus-localized NTA is both necessary and sufficient for pollen tube
304 reception.
305
306
307 **Disrupting the NTA CaMBD compromises NTA's ability to accumulate at the filiform**
308 **apparatus during pollen tube reception**
309 The dramatic differences in protein localization between NTA-GFP and NTA-$MLO1^{CTerm}$-GFP
310 revealed that the C-terminal cytoplasmic domain of NTA contains sequences that cause NTA to
311 be sequestered in the Golgi before pollen tube arrival and possibly also to allow for directed
312 transport to the filiform apparatus in response to signals from the arriving pollen tube. The C-
313 terminal cytoplasmic domains of MLO proteins contain a predicted CaMBD followed by an
314 unconserved tail of variable length [37-39]. A comparison of C-terminal domains (Figure 5A)
315 revealed that NTA and MLO1 share the conserved 20 amino acid 1-8-14 CaM binding motif of

316 hydrophobic residues interspersed with basic residues that define the MLO CaMBD [38], but
317 have different residues surrounding the conserved tryptophan that has been shown to
318 necessary for CaM binding in MLO proteins [38, 39]. In addition, NTA and MLO1 have different
319 length C-terminal tails after the CaMBD (Figure 5A). In order to determine if the C-terminal tail
320 after the CaMBD is necessary for NTA sequestration in the Golgi before pollen tube arrival, we
321 made a GFP fusion with NTA truncated just after the predicted CaMBD ($NTA^{\Delta 481}$, Figure 5A)
322 expressed under control of the synergid-specific MYB98 promoter. This construct
323 complemented the *nta-1* pollen tube reception phenotype and localized in the Golgi before
324 pollen tube arrival (Figure 5C and 5E), revealing that the C-terminal tail after the CaMBD is not
325 necessary for NTA sequestration or function. We next tested whether disruption of the CaMBD
326 would affect NTA localization and/or function. A point mutation in the conserved tryptophan
327 necessary for CaM-binding in other CaMBDs [38, 40, 41] was introduced into our NTA-GFP
328 expression construct (NTA^{W458A}, Figure 5A) and transformed into the *nta-1* background. In
329 contrast to wild-type NTA and $NTA^{\Delta 481}$, which result in an even higher fertility in *nta-1* mutants
330 than in the Ws controls, NTA^{W458A} only partially complemented the *nta-1* fertility phenotype
331 (Figure 5E). Before pollen tube arrival, NTA^{W458A} co-localizes with a Golgi marker in synergids
332 similar to wild-type NTA (Figure 5D and Figure S6). However, during pollen tube reception,
333 NTA^{W458A} displays different accumulation patterns that correlate with the ability of the pollen
334 tube to rupture. In our semi-*in vivo* system, ovules with normal pollen tube rupture had at least
335 partial NTA^{W458A} accumulation at the filiform apparatus, while ovules with pollen tube overgrowth
336 did not accumulate NTA^{W458A} at the filiform apparatus (Figure 6). These data reveal that an
337 intact CaMBD enhances NTA's redistribution to the filiform apparatus during pollen tube
338 reception and that NTA accumulation at the filiform apparatus promotes pollen tube rupture,
339 while the C-terminal tail after the CaMBD is dispensable for NTA function.
340

341 The influence of the CaMBD on NTA accumulation at the filiform apparatus could indicate a
342 connection with the calcium oscillations that occur in synergids during signaling with the arriving
343 pollen tube. The receptor-like kinase FER and the GPI-anchored protein LRE are filiform-
344 localized proteins that interact with each other and form a co-receptor for signals from the
345 arriving pollen tube [14, 16, 17]. *fer* and *lre* mutant ovules fail to initiate synergid calcium
346 oscillations at pollen tube arrival and have highly penetrant pollen tube overgrowth phenotypes
347 [12]. In *nta-1* mutant ovules, synergids have dampened calcium oscillations and around 30% of
348 ovules carrying the mutation display pollen tube overgrowth [12, 13]. In both *fer-1* and *lre-7*
349 backgrounds, NTA-GFP does not accumulate at the filiform apparatus in response to signals
350 from the arriving pollen tube (Figure S8 and [13]), placing NTA accumulation at the filiform
351 apparatus downstream of both FER and LRE and the calcium oscillations conditioned by these
352 proteins.
353

354 **Discussion**

355 **Synergids respond to a signal from the approaching pollen tube**

356 Successful pollination and production of seeds requires a series of signaling events between the
357 male gametophyte (pollen tube) and both sporophytic and gametophytic cells of the female. In
358 this study, we used live imaging to characterize dynamic subcellular changes that occur in the
359 synergid cells of the female gametophyte in response to the arrival of the pollen tube. We
360 showed that both the NTA protein and endosomes are actively mobilized to the filiform
361 apparatus where male-female communication occurs during pollen tube reception (Figure 7).
362 Disrupting the ability of NTA to pass through the secretory system by adding a Golgi retention
363 signal compromised its ability to participate in pollen tube reception, revealing that NTA
364 accumulation at the filiform apparatus is necessary for its function. Mutation of NTA's CaMBD
365 partially compromised NTA redistribution and function in pollen tube reception, revealing that
366 Ca^{2+} may play a role in the synergid response to the signal from the pollen tube.

367

368 The polar accumulation of the RabA1g endosome marker, but not a Golgi marker (Man49-GFP),
369 near the filiform apparatus during pollen tube reception suggests a change in synergid secretory
370 system behavior that is triggered by the approaching pollen tube. Our results with the ER, Golgi,
371 TGN, and peroxisome markers indicate that the mobilization of the RabA1g endosomes toward
372 the approaching pollen tube is not just a symptom of FER signaling triggering synergid cell
373 death that leads to mass disruption of subcellular compartments. Trans-Golgi Network/Early
374 endosomes (TGN/EEs) have been shown to be involved in the trafficking of both secretory and
375 endocytic cargo [42]. RabA1g is present in endosomes that are highly sensitive to Brefeldin A in
376 roots, suggesting that they could function as recycling endosomes [43]. While the resolution of
377 our live imaging system did not allow us to determine whether NTA completely co-localizes with
378 this compartment, it is tempting to speculate that the RabA1g endosomes are mediating the
379 polar movement of NTA to the filiform apparatus. Alternatively, these endosomes could be
380 transporting other signaling molecules either to or from the filiform apparatus.

381

382 **Signal-mediated protein trafficking**

383 Signal-mediated regulation of protein trafficking is an elegant mechanism to control the delivery
384 of molecules to the precise location where they are needed for critical signaling events that
385 occur over relatively short time frames. Selective protein targeting similar to NTA movement in
386 response to pollen tube arrival has also been observed during cell-to-cell communication
387 between the egg and sperm cells in Arabidopsis. After pollen tube reception and release of the
388 sperm cells, a signal from the sperm and/or the degenerated synergid cell causes the egg cell to
389 secrete EGG CELL 1 (EC1) peptides that have been stored in punctate compartments in the
390 egg cytoplasm toward the sperm cells. The sperm cells perceive the EC1 signal and, in turn,
391 mobilize the gamete fusogen HAPLESS2/GENERATIVE CELL SPECIFIC1 (HAP2/GCS1) from
392 a cytoplasmic compartment to the cell surface [44]. This controlled movement of proteins that

393 have already been translated and stored facilitates a quick response to activate the egg and
394 sperm for fertilization. Likewise, NTA mobilization to the filiform apparatus of the synergids as
395 the pollen tube arrives could play a role in sending a signal to the pollen tube that leads to the
396 mobilization of pollen tube proteins that allow the pollen tube to rupture and release the sperm
397 cells. For example, proteins that regulate the integrity of the tip of the pollen tube could be
398 quickly delivered after the "arrival" signal from the synergid is perceived. Recent work on the
399 role of the pollen-expressed ANXUR1 and 2 and BUDDHA PAPER SEAL1 and 2 receptor-like
400 kinases in pollen tube tip integrity support this hypothesis. During pollen tube growth through the
401 female tissues, RALF4 and RALF19 peptides that are secreted from pollen tubes act as ligands
402 for ANX1/2 and BPS1/2 to promote tip growth, while RALF34 secreted from the synergids
403 displaces RALF4 and 19 from the receptors leading to subcellular changes that result in pollen
404 tube rupture [45].
405
406 **Calcium and NTA movement**
407 Our study revealed that an intact CaMBD facilitates the trafficking of NTA from the Golgi to the
408 filiform apparatus in response to a stimulus from the approaching pollen tube. Our live imaging
409 studies and previous reports all suggest that the FER/LRE co-receptor is necessary for
410 perceiving this stimulus and that two other CrRLK1L genes, HERK1 and ANJEA are also
411 necessary for NTA accumulation at the filiform apparatus [13, 46]. Polar accumulation of NTA-
412 GFP at the filiform apparatus occurs in a similar time frame to the FER/LRE-dependent Ca^{2+}_{cyto}
413 spiking in the synergids during pollen tube reception [10, 12]. Subcellular Ca^{2+} spiking occurs in
414 plant responses to both biotic and abiotic external stimuli. Notably, cytosolic Ca^{2+} oscillations
415 occur during pollen tube-synergid interactions, egg-sperm interactions, and in biotrophic
416 interactions between plant cells and both beneficial and harmful microbes (reviewed in [47]). In
417 most cases, the mechanism for decoding Ca^{2+} spikes into a cellular response is not known, but
418 Ca^{2+}-binding proteins such as CaM and CaM-like proteins could play a role in relaying Ca^{2+}

419 signals [48]. In *nta-1* mutants, the cytosolic Ca^{2+} oscillations still occur, but at a lower magnitude
420 than in wild-type synergids, suggesting that NTA could be involved in modulating Ca^{2+} flux [12].
421 A recent study of the pollen tube-expressed MLO5 and MLO9 genes revealed a link between
422 MLO proteins and recruitment of the calcium channel CNGC18 to control Ca^{2+} flux during
423 directional growth [49]. Several CNGC genes are expressed in synergids and could possibly
424 interact with filiform apparatus-localized NTA to regulate the flow of Ca^{2+} ions into or out of the
425 apoplast near the filiform apparatus.
426
427 Calcium has also been linked to regulation of endomembrane trafficking (reviewed in [50]. In
428 animals, CaM plays a role in regulating vesicle tethering and fusion [51], and in plants CaM-like
429 proteins are associated with endosomal populations [52]. Thus, it is possible that the CaMBD in
430 NTA is critical for the precise targeting of NTA in response to pollen tube arrival. Another
431 mechanism that has been proposed for Ca^{2+} regulation of protein targeting is that electrostatic
432 interactions between Ca^{2+} and anionic phospholipids in specific domains of the plasma
433 membrane regulate vesicle fusion and differential recruitment of proteins to these domains [53,
434 54].
435
436 An interesting parallel between powdery mildew infection and pollen tube reception is that in
437 both cases, an MLO protein accumulates at the site of interaction with a tip-growing cell. During
438 powdery mildew infection, active transport of proteins and lipids to penetration site leads to
439 membrane remodeling and establishment of the extrahaustorial membrane (EHM) which
440 separates the plant cytoplasm from the invading fungal hyphae [55]. This specialized membrane
441 is enriched in the anionic phospholipid phosphatidylinositol 4,5 bisphosphate ($PI(4,5)P_2$).
442 Depletion of $PI(4,5)P_2$ in *phosphatidylinositol 4-phosphate 5-kinase 1/2* double mutants (*pip5k1*
443 *pip5k2*) resulted in powdery mildew resistance associated with a failure of MLO2 to accumulate
444 at the EHM in early stages of fungal penetration [56]. Although the composition of the filiform

445 apparatus and its relationship with the arriving pollen tube has not been established, it is
446 possible that similar membrane modification occurs in the filiform apparatus during signaling
447 with the pollen tube and is linked to NTA accumulation at pollen tube arrival.
448
449 **Cell death and pollen tube reception**
450 MLOs were first discovered in barley as powdery mildew resistance genes [57]. *mlo* mutants in
451 both monocots and dicots are resistant to powdery mildew infection, indicating that the MLO
452 proteins are required for infection. These mutants also have ectopic cell death, indicating that
453 one function of MLO proteins is to negatively regulate cell death [58]. Pollen tube reception is
454 catastrophic for both the pollen tube and the receptive synergid cell: both cells die as a result of
455 successful male-female signaling and delivery of the male gametes. The timing of synergid
456 degeneration remains under debate, with some studies suggesting that it occurs upon pollen
457 tube arrival at the synergid and others concluding that it occurs concurrently with pollen tube
458 rupture [31, 59, 60]. Our live imaging experiments with both NTA-GFP and the subcellular
459 compartment reporters suggest that the synergid cells are still alive and regulating their
460 secretory systems up to the point of pollen tube rupture. Given the function of the "powdery
461 mildew" members of the MLO gene family in regulating cell death [61], it is possible that one
462 role of NTA is to prevent early degeneration of the synergids. In both pollen tube reception and
463 powdery mildew infection, an MLO protein might be needed at the site of penetration to stabilize
464 the cell and prevent precocious cell death. Our result that premature delivery of NTA (in the
465 NTA-MLO1^{CTerm} domain swap construct) to the filiform apparatus of the cell does not disrupt
466 pollen tube reception is consistent with this hypothesis, since other signaling processes
467 occurring in the synergids during communication with the arriving pollen tube would likely not be
468 triggered by simply moving NTA to the filiform apparatus in the absence of a pollen tube.
469

470 In this study, we showed that signals from an approaching pollen tube trigger the movement of
471 NTA out of the Golgi and to the filiform apparatus and that this redistribution is necessary for
472 pollen tube reception. Future work will focus on determining the mechanism through which NTA
473 polarly accumulates at the filiform apparatus and on identifying the signals from the pollen tube
474 that lead to important subcellular changes in the synergids during pollen tube reception.
475

476 **Materials and methods**

477 **Plant materials and growth conditions**

478 *Arabidopsis thaliana* lines expressing *NTA$_{pro}$::NTA-GFP*, *MYB98$_{pro}$::NTA-GFP*,
479 *MYB98$_{pro}$::MLO1-GFP*,Golgi-associated marker (Man49-mCherry), ER-associated marker (SP-
480 mCherry-HDEL), TGN-associated marker (SYP61-mCherry), peroxisome-associated marker
481 (Peroxisome-mCherry) and recycling endosome-associated marker (mCherry-RabA1g), were
482 generated and described in previous publications [13, 14, 21, 33]. Pollen tube marker lines,
483 *ACA9::DsRed* [62] and *Lat52::GFP* [28] were generously provided by Dr. Aurelien Boisson-
484 Dernier and Dr. Ravi Palanivelu. *fer-1* seeds were provided by Dr. Ueli Grossniklaus and *lre-7*
485 seeds were provided by Dr. Ravi Palanivelu. Seeds were sterilized and plated on ½-strength
486 Murashige and Skoog (MS) plates. All plates were sealed and stratified at 4˚C for two days, and
487 then transferred to the growth chamber (long day conditions, 16 h of light and 8 h of dark at
488 22˚C) for germination and growth. After 5-7 days, seedlings were transplanted to soil. Seeds
489 from transformed lines were sterilized and plated on ½ MS plate with 20 mg/L hygromycin for
490 selection of transgenic seedlings, which were then transplanted to soil and grown in long days.
491

492 **Live Imaging of Pollination Using a Semi-*in vivo* Pollen Tube Guidance Assay**

493 The semi-*in vivo* system of pollen tube reception was modified from [28]. Approximately 150 µL
494 of pollen germination media (5 mM KCl, 1 mM $MgSO_4$, 0.01% (w/v) H_3BO_3, 5 mM $CaCl_2$, 20%
495 sucrose, 1.5% agarose, and adjusted pH to 7.5 with KOH) was poured into a Glass Bottom
496 Culture Petri Dish (MatTek Corporation, P35G-1.0-20-C) and spread out using a pipette. Pistils
497 were emasculated and 2 d later were hand pollinated with *ACA9::DsRed* or *Lat52::GFP* pollen
498 and returned to the growth chamber. Approximately 1 h after pollination, pistils were removed
499 from plants and placed on double sided tape on a glass slide. Stigmas were cut using single-
500 sided razor blade and placed on pollen germination media using forceps. 8-10 ovules were
501 arranged around the cut style and the petri dish was returned to the growth chamber. After 4-6

502 h, pollen tubes grew through the stigma and style and emerged near the ovules. Imaging
503 commenced when the pollen tubes approached ovules. Time-lapse images were acquired at 5
504 min intervals by spinning disk confocal microscopy using an Andor Revolution XD platform with
505 a Yokogawa CSU-X1-A1 scanner unit mounted on an Olympus IX-83 microscope and a 20X/0.5
506 NA objective (Olympus). An Andor iXon Ultra 897BV EMCCD camera was used to capture GFP
507 fluorescence (488-nm excitation) and red fluorescent protein (dsRed or mCherry) fluorescence
508 (561-nm excitation).
509
510 For each experimental condition, at least 60 ovules were imaged over the time course from
511 pollen tube approaching the ovule to completion of pollen tube reception (pollen tube rupture to
512 release the sperm cells). Neighboring ovules that did not attract pollen tubes were imaged at the
513 same time and served as controls for photoxicity.
514
515 **Confocal laser scanning microscopy (CLSM)**
516 CLSM to examine MLO variant subcellular localization was performed on ovules dissected 2 d
517 after emasculation. FM4-64 staining was performed according to the protocol described in [21].
518 CLSM was done using either a Nikon A1Rsi inverted confocal microscope according to [63] or a
519 Leica SP8 upright confocal microscope according to [21].
520
521 **Quantification of fluorescence signal intensity**
522 Two-channel images were adjusted for brightness and contrast using Fiji [64]. Then, they were
523 input to NIS-Elements software (Ver. 5.02) to measure the fluorescence signal intensity. A line
524 that spanned from the chalazal end to the filiform apparatus end of the synergid was used for
525 the signal intensity measurements. For a more accurate representation of the total area of the
526 synergid, signal intensities were recorded along the same length line at five parallel position

527 within the synergid cell. Finally, all the measurement data were output as Excel files. Graphs
528 and statistical analysis were performed with Prism software (www.graphpad.com).
529
530 **Video processing**
531 Images were filtered to remove the noise and cropped using Fiji (Version 2.0.0). QuickTime
532 Player (Version 10.5) was used for movie editing and time-lapse analyses.
533
534 **Cloning and Generation of Transgenic Lines**
535 PCR amplification with PHUSION High-Fidelity Polymerase (NEB, M0535S) or Q5 High-Fidelity
536 DNA Polymerase (NEB, M0419S) were used to generate the following constructs in this study.
537 Genes were amplified with primers that had attB1 and attB2 sites for recombination via BP
538 reaction into the Gateway-compatible entry vector pDONR207. Full-length NTA entry vectors
539 used in this study was generated as described previously [21] . NTA truncation was amplified
540 using NTA full-length entry vector as a template with forward primer NTA-FattB1 and the
541 reverse primer NTA481-RattB2 (See all primer sequences in Table S1). The NTA^{W458A} point
542 mutation was generated using the same *NTA* template and amplifying two fragments of *NTA*
543 with desired point mutations introduced into the primers: NTA-FattB1 + NTAW458A-R and
544 NTAW458A-F + NTA-RattB2. The two fragments were purified and pasted together with
545 overlaps using a PCR-pasting protocol. The NTA-$MLO1^{CTerm}$ construct was generated using the
546 full-length entry vectors of NTA and MLO1 used in previous study [21] as templates and
547 amplifying two fragments of *NTA* and *MLO1* using the two pairs of primers: NTA-FattB1 +NTA-
548 R19 and MLO1-F + MLO1-RattB2. The two fragments were purified and pasted together with
549 overlaps using a PCR-pasting protocol. The NTA-GFP-RNIKCD construct was generated using
550 the full-length expression vector of $MYB98_{pro}$::NTA-GFP as template. Two separate fragments
551 of NTA and GFP-RNIKCD-1 were amplified with two pairs of primers: NTA-FattB1 + NTA-Gly5-
552 GFP-R and NTA-Gly5-GFP-F + GFP-RNIKCD-RattB2. The two fragments were purified and

553 pasted together with overlaps using a PCR-pasting protocol. The NTA-MLO1^{CTerm}-GFP-RNIKCD
554 construct was generated using the full-length expression vector of MYB98$_{pro}$::NTA-MLO1^{CTerm}-
555 GFP as template and two fragments of NTA-MLO1^{CTerm} and GFP-RNIKCD-2 were amplified
556 using the two pairs of primers: NTA-FattB1 + MLO1-Gly5-GFP-R and MLO1-Gly5-GFP-F +
557 GFP-RNIKCD-RattB2. The two fragments were purified and pasted together with overlaps using
558 a PCR-pasting protocol. The coding sequence from the truncation and the point mutation and
559 the fusion sequences were fully sequenced in entry vectors. NTA$^{\Delta 481}$ and NTA^{W458A} entries were
560 then recombined via LR reactions into the pMDC83 backbone with the MYB98$_{pro}$ [65] to drive
561 expression of each NTA variant in synergid cells with a C-terminal GFP fusion and NTA-GFP-
562 RNIKCD and NTA-MLO1^{CTerm}-GFP-RNIKCD entries were then recombined via LR reactions into
563 pMDC32 plasmids with the MYB98$_{pro}$ for synergid expression and FER$_{pro}$ for tobacco transient
564 expression.
565
566 For *nta-1* complementation assay and co-localization analyses, expression vectors were
567 transformed into the *Agrobacterium tumefaciens* strain GV3101 and transformed into the *nta-1*
568 mutant background or the Col-0 background (for co-localization combinations, Col-0 stably
569 expressing the Golgi or TGN synergid secretory markers was used for transformation) via the
570 floral-dip method [66]. Stable transgenic lines were selected using their respective selections
571 described above. Homozygous T2 or T3 lines were used in *nta-1* complementation assay and
572 co-localization imaging in the synergid was done in a T1 or T2 analysis. The NTA$_{pro}$::NTA-GFP
573 construct described in [13] was introduced into the *lre-7* background by floral dip as described
574 above.
575
576 ***nta-1* Complementation Assays**
577 2-4 independent insertion lines for each construct were taken to the T2 generation and
578 screened for homozygosity using fluorescence microscopy to ensure transgene expression in

synergids of every ovule. Unfertilized vs. fertilized ovule counts from self-pollinated flowers were assessed in at least five plants of each insertion line and compared to *nta-1*, Wassilewskija (Ws-2; wildtype), and the previously published full-length NTA ($MYB98_{pro}$::NTA-GFP in *nta-1* background, [21]. Ovule counts were statistically analyzed using Prism with significance determined using a Student's *t*-test. Comparisons of the NTA variants were made to full-length NTA and the *nta-1* mutant.

Acknowledgements

We thank Patrick Day for technical assistance and Rachel Flynn and Thomas Davis for helpful discussions and comments on the manuscript. This work was supported by funds from NSF IOS-1733865 to SAK, Purdue University Start-up funds to SAK, and a grant from the Oklahoma Center for the Advancement of Science and Technology #PS14-008 to SAK. Spinning disk confocal microscopy in the Staiger laboratory was supported, in part, by an award from the Office of Science at the US Department of Energy, Physical Biosciences Program, under contract number DE-FG02-09ER15526 to CJS.

Author Contributions

JY, YJ, DSJ, and SAK conceived and designed the experiments. JY, YJ, DSJ, NL, and WZ performed the experiments. JY, YJ, DSJ, and SAK analyzed the data. JY, YJ, DSJ, and SAK wrote the manuscript, and all authors revised and approved the final manuscript.

Competing Interests

The authors declare no competing interests.

605

606 **Figure Legends**

607 **Figure 1. NTA-GFP accumulates at the filiform apparatus as the pollen tube approaches.**
608 (A) Diagram of a mature *Arabidopsis thaliana* ovule and embryo sac, modified from Jones et al,
609 2018. CC, Central Cell; Syn, Synergid Cells; EC, Egg Cell; An, Antipodal cells; FA, Filiform
610 Apparatus (B, C) Live imaging of pollen tube (PT) reception using NTA-GFP labeled synergids
611 (green signal) and *ACA9::DsRed* pollen tubes (magenta signal). (B) Polar NTA-GFP
612 accumulation at the filiform apparatus (FA) occurred in ovules that attracted a pollen tube
613 (ovules with yellow stars), while polar NTA-GFP accumulation did not occur in ovules without
614 pollen tube attraction (ovules with white stars). (C) Time-lapse imaging of NTA-GFP
615 accumulation during pollen tube reception. (D) Quantification of NTA-GFP signal along the
616 length of the synergid from chalazal end (0μm) to FA end (33μm) at 0min, 25min, 50min, 75min,
617 and 100min timepoints, respectively. (E) 6 more examples of the quantification of NTA-GFP
618 signal along the length of synergids after pollen tube arrival. (F) Quantification of the percentage
619 of ovules with different NTA accumulation patterns under the same imaging conditions. Bars=50
620 μm (B and C).

621

622 **Figure 2. The Golgi marker is randomly distributed throughout synergids during pollen**
623 **tube reception.** (A) NTA-GFP (green signal) and Golgi-mCherry signals (magenta signal) are
624 evenly distributed along the length of the synergid and co-localized within synergid cells before
625 pollen tube arrival. (B) After pollen tube arrival, NTA-GFP accumulated at the FA, but Golgi-
626 mCherry did not accumulate at the FA. (C) Live imaging of Golgi-mCherry during reception of
627 *Lat52::GFP* labeled pollen tubes. (D) Quantification of Golgi-mCherry signal along the length of
628 synergids shown in (C) before and after pollen tube arrival. Bars=30μm (A-B), 50μm (C).

629

630 **Figure 3. RabA1g endosomes polarly accumulate toward the filiform apparatus during**
631 **pollen tube reception.** (A) RabA1g-mCherry endosome marker (magenta signal) accumulates
632 at the FA region in response to pollen tube arrival (ovule with yellow star). The ovule with no
633 pollen tube attraction (white star) serves as a negative control imaged under the same
634 conditions. (B) Higher magnification of the micropylar region of starred ovule in (red box in panel
635 A). (C) Timing of RabA1g-mCherry polar accumulation during pollen tube arrival. Bars=50μm.
636 (D) Quantification of RabA1g-mCherry signal along the length of synergids during pollen tube
637 reception. Synergid cell from chalazal end to filiform apparatus (FA) end was defined from 0 to
638 33 μm in length. (E) 6 more examples of the quantification of RabA1g-mCherry signal after
639 pollen tube arrival. (F) Quantification of ovule percentage with RabA1g endosome marker
640 throughout the synergids (gray bars) or with polar accumulation at or near the filiform apparatus
641 (black bars).
642
643 **Figure 4. Targeting of NTA to the filiform apparatus before pollen tube arrival is not toxic**
644 **to synergid cells.** (A-E) Localization patterns of MYB98 promoter driven MLO-GFP variants
645 (green signal) in synergids of mature virgin ovules stained with FM4-64 (magenta signal) to reveal
646 the outline of the synergid and the filiform apparatus (FA, diffuse magenta signal). Graphs in each
647 panel show quantification of the GFP intensity of the MLO variants along the length of the
648 synergids. Bars = 10 μm. (F) Percentage of ovules showing MLO-GFP signal throughout the
649 synergids (100% of length), in the FA only (20% of length) and the region surrounding and
650 including the FA (40% of length). (F) Scatter plot of unfertilized ovule percentages in homozygous
651 plants of pMYB98::MLO-GFP in *nta-1* mutants to assess the ability of the MLO-GFP constructs
652 to complement *nta-1*. WS, Wassilewskija. Significance was determined by a Student's *t*-test (****,
653 $P < 0.0001$; *, $P = 0.0281$; and ns, $P = 0.2020$).
654
655

656 **Figure 5. Analysis of NTA variants expressed in synergids of *nta-1*.** (A) Alignment of MLO1
657 and NTA C-terminal domains after the seventh membrane span. Red bars highlight the CaMBD;
658 W458A and Δ481 indicate the point mutation in NTA and the deletion point, respectively ; a.a.,
659 amino acid. (B-D) NTA (variant)-GFP (green) distribution in synergid cells of unfertilized ovules
660 stained with FM4-64 (magenta signal). Bar = 10 µm. (E) Complementation analysis of NTA
661 variants in T2 plants homozygous for $MYB98_{pro}$::NTA(variant)-GFP constructs in *nta-1* mutants.
662 Adjusted P values from a Student's *t*-test are as follows: **** indicates $P < 0.0001$; *** indicates
663 $P = 0.001$ to 0.0001; and ns indicates $P > 0.05$.
664
665 **Figure 6. A point mutation in the CaMBD (NTA^{W458A}) affects filiform apparatus**
666 **accumulation of NTA and pollen tube reception.** (A) NTA^{W458A}-GFP has 3 different
667 localization patterns in response to PT arrival under semi *in-vivo* conditions. Bar=50 µm (B)
668 Quantification of GFP signal intensity in NTA^{W458A} synergids during pollen tube reception. (C)
669 Analysis of NTA^{W458A}-GFP distribution patterns in ovules with successful (PT bursting) and
670 unsuccessful (no PT or PT overgrowth (PT OG)) pollen tube reception.
671
672 **Figure 7. Subcellular dynamics in synergids during pollen tube reception.** (A) Pollination
673 using a semi-*in vivo* pollen tube guidance assay. (B) Before pollen tube arrival, NTA is in a
674 Golgi-associated compartment and RabA1g endosomes are distributed throughout the
675 synergids. (C) As a pollen tube arrives, NTA and RabA1g endosomes move toward the filiform
676 apparatus (FA). NTA accumulation is dependent on signaling from the FER receptor like kinase,
677 which acts in a complex with LRE. Abbreviations: CC, Central Cell; Syn, Synergid cells; EC,
678 Egg Cell; An, Antipodal cells; nuc, Nucleus; FA, Filiform Apparatus.
679
680
681 **Supplemental Materials**

682 **Supplementary figure 1.** NTA-GFP does not polarly accumulate at the filiform apparatus in
683 synergids without pollen tube attraction.
684 **Supplementary figure 2.** Peroxisomes do not exhibit polar accumulation at the filiform
685 apparatus during pollen tube reception.
686 **Supplementary figure 3.** Trans-Golgi marker distribution in synergids does not change in
687 response to pollen tube reception.
688 **Supplementary figure 4.** ER marker distribution in synergids does not change in response to
689 pollen tube reception.
690 **Supplementary figure 5**. Additional examples of the polar accumulation of RabA1g endosomes
691 during pollen tube reception.
692 **Supplementary figure 6.** NTA^{W458A} co-localizes with Golgi marker in synergid cells before pollen
693 tube arrival.
694 **Supplementary figure 7**. A C-terminal Golgi retention signal retains MLO1 and NTA variants in
695 the Golgi.
696 **Supplementary figure 8**. NTA-GFP polar accumulation requires FER and LRE.
697
698 **Supplemental Movies**
699 **Supplementary movie 1.** NTA-GFP (green signal) accumulates at the filiform apparatus as
700 ACA9::DsRed labeled pollen tube (magenta signal) approaches.
701 **Supplementary movie 2.** NTA-GFP (green signal) accumulates at the filiform apparatus during
702 pollen tube reception (GFP channel only, same movie as S1).
703 **Supplementary movie 3.** Golgi-mCherry signals (magenta signal) are evenly distributed along
704 the length of the synergid as Lat52::GFP labeled pollen tube (green signal) approaches.

705 **Supplementary movie 4.** Golgi-mCherry signals (magenta signal) are evenly distributed along
706 the length of the synergid during pollen tube reception (mCherry channel only, same movie as
707 S3).
708 **Supplementary movie 5.** The trans-Golgi marker SYP61-mCherry (magenta signal) is localized
709 toward the micropylar region of synergid cells both before and after pollen tube (green signal)
710 arrival.
711 **Supplementary movie 6.** The trans-Golgi marker SYP61-mCherry (magenta signal) is localized
712 toward the micropylar region of synergid cells during pollen tube reception (mCherry channel
713 only, same movie as S5).
714 **Supplementary movie 7.** Before and after pollen tube (green signal) arrival, the ER marker SP-
715 mCherry-HDEL (magenta signal) is distributed throughout synergid cells.
716 **Supplementary movie 8.** The ER marker SP-mCherry-HDEL (magenta signal) is distributed
717 throughout synergid cells (mCherry channel only, same movie as S7).
718 **Supplementary movie 9.** The peroxisome marker mCherry-SLK (magenta signal) does not
719 accumulate at the filiform apparatus after pollen tube (green signal) arrival.
720 **Supplementary movie 10.** The peroxisome marker mCherry-SLK (magenta signal) does not
721 accumulate at the filiform apparatus during pollen tube reception (mCherry channel only, same
722 movie as S9).
723 **Supplementary movie 11.** RabA1g-mCherry endosome marker (magenta signal) accumulates
724 at the filiform apparatus in response to pollen tube (green signal) arrival.
725 **Supplementary movie 12.** RabA1g-mCherry endosome marker (magenta signal) accumulates
726 at the filiform apparatus in response to pollen tube (green signal) arrival (mCherry channel only,
727 same movie as S11).
728
729
730

731 **References**

732 1. Naramoto, S. (2017). Polar transport in plants mediated by membrane transporters:
733 focus on mechanisms of polar auxin transport. Curr Opin Plant Biol *40*, 8-14.
734 2. Petrasek, J., Mravec, J., Bouchard, R., Blakeslee, J.J., Abas, M., Seifertova, D.,
735 Wisniewska, J., Tadele, Z., Kubes, M., Covanova, M., et al. (2006). PIN proteins perform a
736 rate-limiting function in cellular auxin efflux. Science *312*, 914-918.
737 3. Salanenka, Y., Verstraeten, I., Lofke, C., Tabata, K., Naramoto, S., Glanc, M., and Friml, J.
738 (2018). Gibberellin DELLA signaling targets the retromer complex to redirect protein
739 trafficking to the plasma membrane. Proc Natl Acad Sci U S A *115*, 3716-3721.
740 4. Johnson, M.A., Harper, J.F., and Palanivelu, R. (2019). A Fruitful Journey: Pollen Tube
741 Navigation from Germination to Fertilization. Annu Rev Plant Biol.
742 5. Drews, G.N., and Yadegari, R. (2002). Development and function of the angiosperm
743 female gametophyte. Annu Rev Genet *36*, 99-124.
744 6. Takeuchi, H., and Higashiyama, T. (2016). Tip-localized receptors control pollen tube
745 growth and LURE sensing in Arabidopsis. Nature *531*, 245-248.
746 7. Wang, T., Liang, L., Xue, Y., Jia, P.F., Chen, W., Zhang, M.X., Wang, Y.C., Li, H.J., and Yang,
747 W.C. (2016). A receptor heteromer mediates the male perception of female attractants
748 in plants. Nature *531*, 241-244.
749 8. Okuda, S., Tsutsui, H., Shiina, K., Sprunck, S., Takeuchi, H., Yui, R., Kasahara, R.D.,
750 Hamamura, Y., Mizukami, A., Susaki, D., et al. (2009). Defensin-like polypeptide LUREs
751 are pollen tube attractants secreted from synergid cells. Nature *458*, 357-361.
752 9. Kessler, S.A., and Grossniklaus, U. (2011). She's the boss: signaling in pollen tube
753 reception. Curr Opin Plant Biol *14*, 622-627.
754 10. Denninger, P., Bleckmann, A., Lausser, A., Vogler, F., Ott, T., Ehrhardt, D.W., Frommer,
755 W.B., Sprunck, S., Dresselhaus, T., and Grossmann, G. (2014). Male-female
756 communication triggers calcium signatures during fertilization in Arabidopsis. Nature
757 communications *5*, 4645.
758 11. Iwano, M., Ngo, Q.A., Entani, T., Shiba, H., Nagai, T., Miyawaki, A., Isogai, A.,
759 Grossniklaus, U., and Takayama, S. (2012). Cytoplasmic Ca2+ changes dynamically during
760 the interaction of the pollen tube with synergid cells. Development *139*, 4202-4209.
761 12. Ngo, Q.A., Vogler, H., Lituiev, D.S., Nestorova, A., and Grossniklaus, U. (2014). A Calcium
762 Dialog Mediated by the FERONIA Signal Transduction Pathway Controls Plant Sperm
763 Delivery. Dev Cell *29*, 491-500.
764 13. Kessler, S.A., Shimosato-Asano, H., Keinath, N.F., Wuest, S.E., Ingram, G., Panstruga, R.,
765 and Grossniklaus, U. (2010). Conserved molecular components for pollen tube reception
766 and fungal invasion. Science *330*, 968-971.
767 14. Liu, X., Castro, C., Wang, Y., Noble, J., Ponvert, N., Bundy, M., Hoel, C., Shpak, E., and
768 Palanivelu, R. (2016). The Role of LORELEI in Pollen Tube Reception at the Interface of
769 the Synergid Cell and Pollen Tube Requires the Modified Eight-Cysteine Motif and the
770 Receptor-Like Kinase FERONIA. Plant Cell *28*, 1035-1052.
771 15. Capron, A., Gourgues, M., Neiva, L.S., Faure, J.E., Berger, F., Pagnussat, G., Krishnan, A.,
772 Alvarez-Mejia, C., Vielle-Calzada, J.P., Lee, Y.R., et al. (2008). Maternal Control of Male-

773 Gamete Delivery in Arabidopsis Involves a Putative GPI-Anchored Protein Encoded by
774 the LORELEI Gene. Plant Cell *20*, 3038-3049.
775 16. Li, C., Yeh, F.L., Cheung, A.Y., Duan, Q., Kita, D., Liu, M.C., Maman, J., Luu, E.J., Wu, B.W.,
776 Gates, L., et al. (2015). Glycosylphosphatidylinositol-anchored proteins as chaperones
777 and co-receptors for FERONIA receptor kinase signaling in Arabidopsis. Elife *4*.
778 17. Escobar-Restrepo, J.M., Huck, N., Kessler, S., Gagliardini, V., Gheyselinck, J., Yang, W.C.,
779 and Grossniklaus, U. (2007). The FERONIA receptor-like kinase mediates male-female
780 interactions during pollen tube reception. Science *317*, 656-660.
781 18. Devoto, A., Hartmann, H.A., Piffanelli, P., Elliott, C., Simmons, C., Taramino, G., Goh, C.S.,
782 Cohen, F.E., Emerson, B.C., Schulze-Lefert, P., et al. (2003). Molecular phylogeny and
783 evolution of the plant-specific seven-transmembrane MLO family. J Mol Evol *56*, 77-88.
784 19. Kusch, S., Pesch, L., and Panstruga, R. (2016). Comprehensive Phylogenetic Analysis
785 Sheds Light on the Diversity and Origin of the MLO Family of Integral Membrane
786 Proteins. Genome Biol Evol *8*, 878-895.
787 20. Yang, T., and Poovaiah, B. (2003). Calcium/calmodulin-mediated signal network in
788 plants. Trends in plant science *8*, 505-512.
789 21. Jones, D.S., Yuan, J., Smith, B.E., Willoughby, A.C., Kumimoto, E.L., and Kessler, S.A.
790 (2017). MILDEW RESISTANCE LOCUS O Function in Pollen Tube Reception Is Linked to Its
791 Oligomerization and Subcellular Distribution. Plant Physiol *175*, 172-185.
792 22. Lindner, H., Kessler, S.A., Müller, L.M., Shimosato-Asano, H., Boisson-Dernier, A., and
793 Grossniklaus, U. (2015). TURAN and EVAN mediate pollen tube reception in Arabidopsis
794 synergids through protein glycosylation. PLoS Biol *13*, e1002139.
795 23. Huck, N., Moore, J.M., Federer, M., and Grossniklaus, U. (2003). The Arabidopsis mutant
796 feronia disrupts the female gametophytic control of pollen tube reception.
797 Development *130*, 2149-2159.
798 24. Rotman, N., Rozier, F., Boavida, L., Dumas, C., Berger, F., and Faure, J.E. (2003). Female
799 control of male gamete delivery during fertilization in Arabidopsis thaliana. Curr Biol *13*,
800 432-436.
801 25. Mansfield, S.G., Briarty, L.G., and Erni, S. (1991). Early embryogenesis in Arabidopsis
802 thaliana. I. The mature embryo sac. Canadian Journal of Botany *69*, 447-460.
803 26. Huang, B.-Q., and Russell, S.D. (1992). Female Germ Unit: Organization, Isolation, and
804 Function. *140*, 233-293.
805 27. Leshem, Y., Johnson, C., and Sundaresan, V. (2013). Pollen tube entry into the synergid
806 cell of Arabidopsis is observed at a site distinct from the filiform apparatus. Plant
807 reproduction *26*, 93-99.
808 28. Palanivelu, R., and Preuss, D. (2006). Distinct short-range ovule signals attract or repel
809 Arabidopsis thaliana pollen tubes in vitro. BMC Plant Biol *6*, 7.
810 29. Hamamura, Y., Nishimaki, M., Takeuchi, H., Geitmann, A., Kurihara, D., and Higashiyama,
811 T. (2014). Live imaging of calcium spikes during double fertilization in Arabidopsis. Nat
812 Commun *5*, 4722.
813 30. Hamamura, Y., Nagahara, S., and Higashiyama, T. (2012). Double fertilization on the
814 move. Curr Opin Plant Biol *15*, 70-77.
815 31. Hamamura, Y., Saito, C., Awai, C., Kurihara, D., Miyawaki, A., Nakagawa, T., Kanaoka,
816 M.M., Sasaki, N., Nakano, A., Berger, F., et al. (2011). Live-cell imaging reveals the

817 dynamics of two sperm cells during double fertilization in Arabidopsis thaliana. Curr Biol
818 *21*, 497-502.
819 32. Huang, J., Ju, Y., Wang, X., Zhang, Q., and Sodmergen (2015). A one-step rectification of
820 sperm cell targeting ensures the success of double fertilization. J Integr Plant Biol *57*,
821 496-503.
822 33. Jones, D.S., Liu, X., Willoughby, A.C., Smith, B.E., Palanivelu, R., and Kessler, S.A. (2018).
823 Cellular distribution of secretory pathway markers in the haploid synergid cells of
824 Arabidopsis thaliana. Plant J *94*, 192-202.
825 34. Stoorvogel, W., Strous, G.J., Geuze, H.J., Oorschot, V., and Schwartz, A.L. (1991). Late
826 endosomes derive from early endosomes by maturation. Cell *65*, 417-427.
827 35. Jones, D.S., and Kessler, S.A. (2017). Cell type-dependent localization of MLO proteins.
828 Plant Signal Behav *12*.
829 36. Gao, C., Yu, C.K., Qu, S., San, M.W., Li, K.Y., Lo, S.W., and Jiang, L. (2012). The Golgi-
830 localized Arabidopsis endomembrane protein12 contains both endoplasmic reticulum
831 export and Golgi retention signals at its C terminus. Plant Cell *24*, 2086-2104.
832 37. Devoto, A., Piffanelli, P., Nilsson, I., Wallin, E., Panstruga, R., von Heijne, G., and Schulze-
833 Lefert, P. (1999). Topology, subcellular localization, and sequence diversity of the Mlo
834 family in plants. J Biol Chem *274*, 34993-35004.
835 38. Kim, M.C., Lee, S.H., Kim, J.K., Chun, H.J., Choi, M.S., Chung, W.S., Moon, B.C., Kang,
836 C.H., Park, C.Y., Yoo, J.H., et al. (2002). Mlo, a modulator of plant defense and cell death,
837 is a novel calmodulin-binding protein. Isolation and characterization of a rice Mlo
838 homologue. J Biol Chem *277*, 19304-19314.
839 39. Kim, M.C., Panstruga, R., Elliott, C., Muller, J., Devoto, A., Yoon, H.W., Park, H.C., Cho,
840 M.J., and Schulze-Lefert, P. (2002). Calmodulin interacts with MLO protein to regulate
841 defence against mildew in barley. Nature *416*, 447-451.
842 40. Arazi, T., Baum, G., Snedden, W.A., Shelp, B.J., and Fromm, H. (1995). Molecular and
843 Biochemical-Analysis of Calmodulin Interactions with the Calmodulin-Binding Domain of
844 Plant Glutamate-Decarboxylase. Plant Physiology *108*, 551-561.
845 41. Yamada, M., Miyawaki, A., Saito, K., Nakajima, T., Yamamoto-Hino, M., Ryo, Y., Furuichi,
846 T., and Mikoshiba, K. (1995). The calmodulin-binding domain in the mouse type 1
847 inositol 1,4,5-trisphosphate receptor. Biochem J *308 (Pt 1)*, 83-88.
848 42. Viotti, C., Bubeck, J., Stierhof, Y.D., Krebs, M., Langhans, M., van den Berg, W., van
849 Dongen, W., Richter, S., Geldner, N., Takano, J., et al. (2010). Endocytic and secretory
850 traffic in Arabidopsis merge in the trans-Golgi network/early endosome, an independent
851 and highly dynamic organelle. Plant Cell *22*, 1344-1357.
852 43. Geldner, N., Denervaud-Tendon, V., Hyman, D.L., Mayer, U., Stierhof, Y.D., and Chory, J.
853 (2009). Rapid, combinatorial analysis of membrane compartments in intact plants with a
854 multicolor marker set. Plant J *59*, 169-178.
855 44. Sprunck, S., Rademacher, S., Vogler, F., Gheyselinck, J., Grossniklaus, U., and
856 Dresselhaus, T. (2012). Egg cell-secreted EC1 triggers sperm cell activation during double
857 fertilization. Science *338*, 1093-1097.
858 45. Ge, Z., Bergonci, T., Zhao, Y., Zou, Y., Du, S., Liu, M.C., Luo, X., Ruan, H., Garcia-Valencia,
859 L.E., Zhong, S., et al. (2017). Arabidopsis pollen tube integrity and sperm release are
860 regulated by RALF-mediated signaling. Science *358*, 1596-1600.

861 46. Galindo-Trigo, S., Blanco-Tourinan, N., DeFalco, T.A., Wells, E.S., Gray, J.E., Zipfel, C., and
862 Smith, L.M. (2020). CrRLK1L receptor-like kinases HERK1 and ANJEA are female
863 determinants of pollen tube reception. EMBO Rep *21*, e48466.
864 47. Chen, J., Gutjahr, C., Bleckmann, A., and Dresselhaus, T. (2015). Calcium signaling during
865 reproduction and biotrophic fungal interactions in plants. Mol Plant *8*, 595-611.
866 48. Chin, D., and Means, A.R. (2000). Calmodulin: a prototypical calcium sensor. Trends Cell
867 Biol *10*, 322-328.
868 49. Meng, J.G., Liang, L., Jia, P.F., Wang, Y.C., Li, H.J., and Yang, W.C. (2020). Integration of
869 ovular signals and exocytosis of a Ca(2+) channel by MLOs in pollen tube guidance. Nat
870 Plants *6*, 143-153.
871 50. Himschoot, E., Pleskot, R., Van Damme, D., and Vanneste, S. (2017). The ins and outs of
872 Ca(2+) in plant endomembrane trafficking. Curr Opin Plant Biol *40*, 131-137.
873 51. Burgoyne, R.D., and Clague, M.J. (2003). Calcium and calmodulin in membrane fusion.
874 Biochim Biophys Acta *1641*, 137-143.
875 52. Ruge, H., Flosdorff, S., Ebersberger, I., Chigri, F., and Vothknecht, U.C. (2016). The
876 calmodulin-like proteins AtCML4 and AtCML5 are single-pass membrane proteins
877 targeted to the endomembrane system by an N-terminal signal anchor sequence. J Exp
878 Bot *67*, 3985-3996.
879 53. Platre, M.P., Noack, L.C., Doumane, M., Bayle, V., Simon, M.L.A., Maneta-Peyret, L.,
880 Fouillen, L., Stanislas, T., Armengot, L., Pejchar, P., et al. (2018). A Combinatorial Lipid
881 Code Shapes the Electrostatic Landscape of Plant Endomembranes. Dev Cell *45*, 465-480
882 e411.
883 54. Simon, M.L., Platre, M.P., Marques-Bueno, M.M., Armengot, L., Stanislas, T., Bayle, V.,
884 Caillaud, M.C., and Jaillais, Y. (2016). A PtdIns(4)P-driven electrostatic field controls cell
885 membrane identity and signalling in plants. Nat Plants *2*, 16089.
886 55. Huckelhoven, R., and Panstruga, R. (2011). Cell biology of the plant-powdery mildew
887 interaction. Curr Opin Plant Biol *14*, 738-746.
888 56. Qin, L., Zhou, Z., Li, Q., Zhai, C., Liu, L., Quilichini, T.D., Gao, P., Kessler, S.A., Jaillais, Y.,
889 Datla, R., et al. (2020). Specific Recruitment of Phosphoinositide Species to the Plant-
890 Pathogen Interfacial Membrane Underlies Arabidopsis Susceptibility to Fungal Infection.
891 Plant Cell.
892 57. Buschges, R., Hollricher, K., Panstruga, R., Simons, G., Wolter, M., Frijters, A., van
893 Daelen, R., van der Lee, T., Diergaarde, P., Groenendijk, J., et al. (1997). The barley Mlo
894 gene: a novel control element of plant pathogen resistance. Cell *88*, 695-705.
895 58. Panstruga, R. (2005). Serpentine plant MLO proteins as entry portals for powdery
896 mildew fungi. Biochem Soc Trans *33*, 389-392.
897 59. Leydon, A.R., Tsukamoto, T., Dunatunga, D., Qin, Y., Johnson, M.A., and Palanivelu, R.
898 (2015). Pollen Tube Discharge Completes the Process of Synergid Degeneration That Is
899 Initiated by Pollen Tube-Synergid Interaction in Arabidopsis. Plant Physiol *169*, 485-496.
900 60. Sandaklie-Nikolova, L., Palanivelu, R., King, E.J., Copenhaver, G.P., and Drews, G.N.
901 (2007). Synergid cell death in Arabidopsis is triggered following direct interaction with
902 the pollen tube. Plant Physiol *144*, 1753-1762.

903 61. Piffanelli, P., Zhou, F., Casais, C., Orme, J., Jarosch, B., Schaffrath, U., Collins, N.C.,
904 Panstruga, R., and Schulze-Lefert, P. (2002). The barley MLO modulator of defense and
905 cell death is responsive to biotic and abiotic stress stimuli. Plant Physiol *129*, 1076-1085.
906 62. Boisson-Dernier, A., Frietsch, S., Kim, T.H., Dizon, M.B., and Schroeder, J.I. (2008). The
907 peroxin loss-of-function mutation abstinence by mutual consent disrupts male-female
908 gametophyte recognition. Curr Biol *18*, 63-68.
909 63. Yuan, J., and Kessler, S.A. (2019). A genome-wide association study reveals a novel
910 regulator of ovule number and fertility in Arabidopsis thaliana. PLoS Genet *15*,
911 e1007934.
912 64. Schindelin, J., Arganda-Carreras, I., Frise, E., Kaynig, V., Longair, M., Pietzsch, T.,
913 Preibisch, S., Rueden, C., Saalfeld, S., Schmid, B., et al. (2012). Fiji: an open-source
914 platform for biological-image analysis. Nat Methods *9*, 676-682.
915 65. Muller, L.M., Lindner, H., Pires, N.D., Gagliardini, V., and Grossniklaus, U. (2016). A
916 subunit of the oligosaccharyltransferase complex is required for interspecific
917 gametophyte recognition in Arabidopsis. Nat Commun *7*, 10826.
918 66. Bent, A. (2006). Arabidopsis thaliana Floral Dip Transformation Method. In Methods in
919 Molecular Biology, Volume 343, K. Wang, ed. (Totowa, NJ: Humana Press Inc.).
920

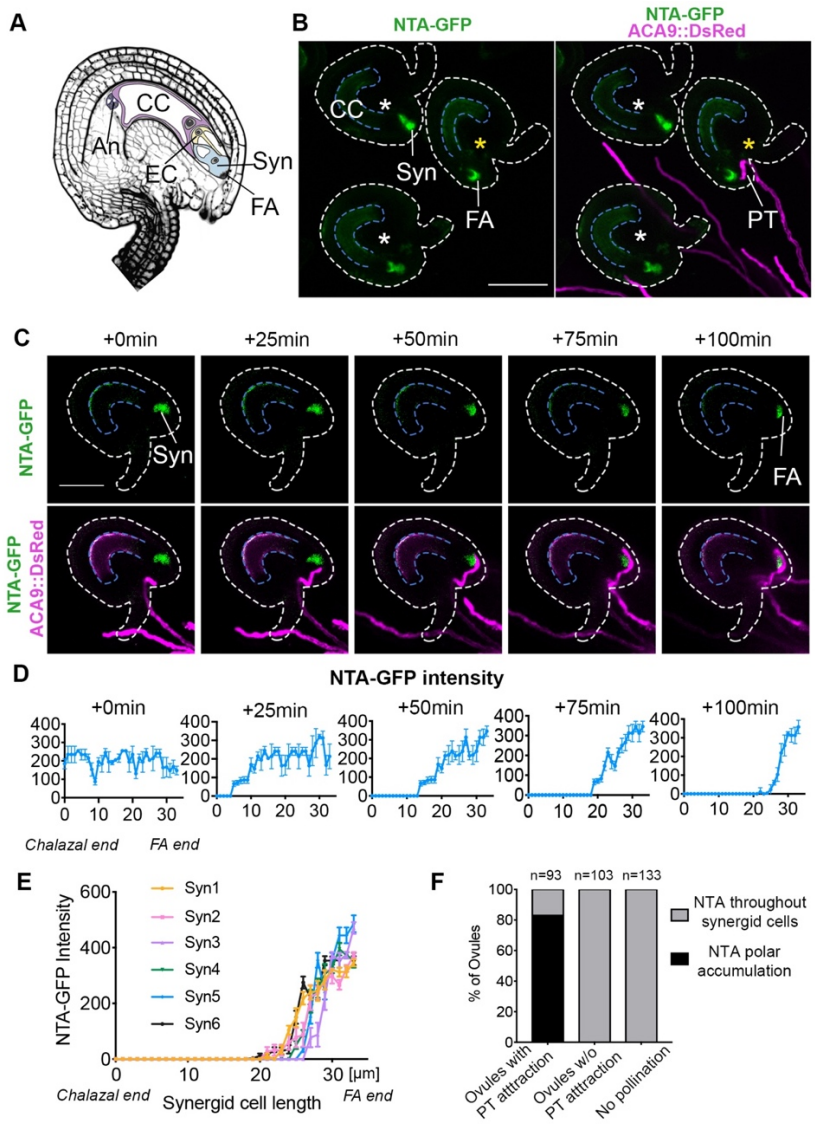

Figure 1. NTA-GFP accumulates at the filiform apparatus as the pollen tube approaches. (A) Diagram of a mature *Arabidopsis thaliana* ovule and embryo sac, modified from Jones et al, 2018. CC, Central Cell; Syn, Synergid Cells; EC, Egg Cell; An, Antipodal cells; FA, Filiform Apparatus (B, C) Live imaging of pollen tube (PT) reception using NTA-GFP labeled synergids (green signal) and ACA9::DsRed pollen tubes (magenta signal). (B) Polar NTA-GFP accumulation at the filiform apparatus (FA) occurred in ovules that attracted a pollen tube (ovules with yellow stars), while polar NTA-GFP accumulation did not occur in ovules without pollen tube attraction (ovules with white stars). (C) Time-lapse imaging of NTA-GFP accumulation during pollen tube reception. (D) Quantification of NTA-GFP signal along the length of the synergid from chalazal end (0μm) to FA end (33μm) at 0min, 25min, 50min, 75min, and 100min timepoints, respectively. (E) 6 more examples of the quantification of NTA-GFP signal along the length of synergids after pollen tube arrival. (F) Quantification of the percentage of ovules with different NTA accumulation patterns under the same imaging conditions. Bars=50 μm (B and C).

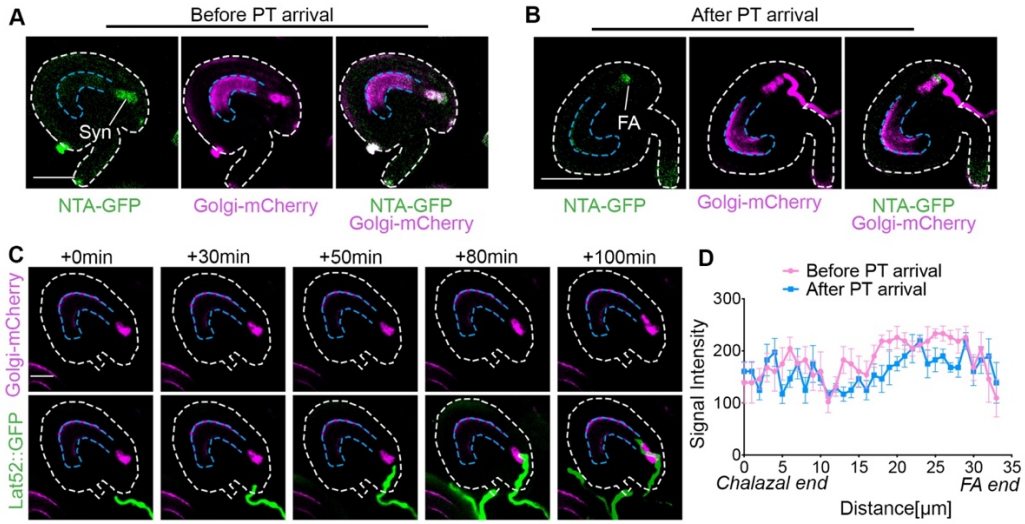

Figure 2. A Golgi marker is randomly distributed throughout synergids during pollen tube reception. (A) NTA-GFP (green signal) and Golgi-mCherry signals (magenta signal) are evenly distributed along the length of the synergid and co-localized within synergid cells before pollen tube arrival. (B) After pollen tube arrival, NTA-GFP accumulated at the FA, but Golgi-mCherry did not accumulate at the FA. (C) Live imaging of Golgi-mCherry during reception of Lat52::GFP labeled pollen tubes. (D) Quantification of Golgi-mCherry signal along the length of synergids shown in (C) before and after pollen tube arrival. Bars=30μm (A-B), 50μm (C).

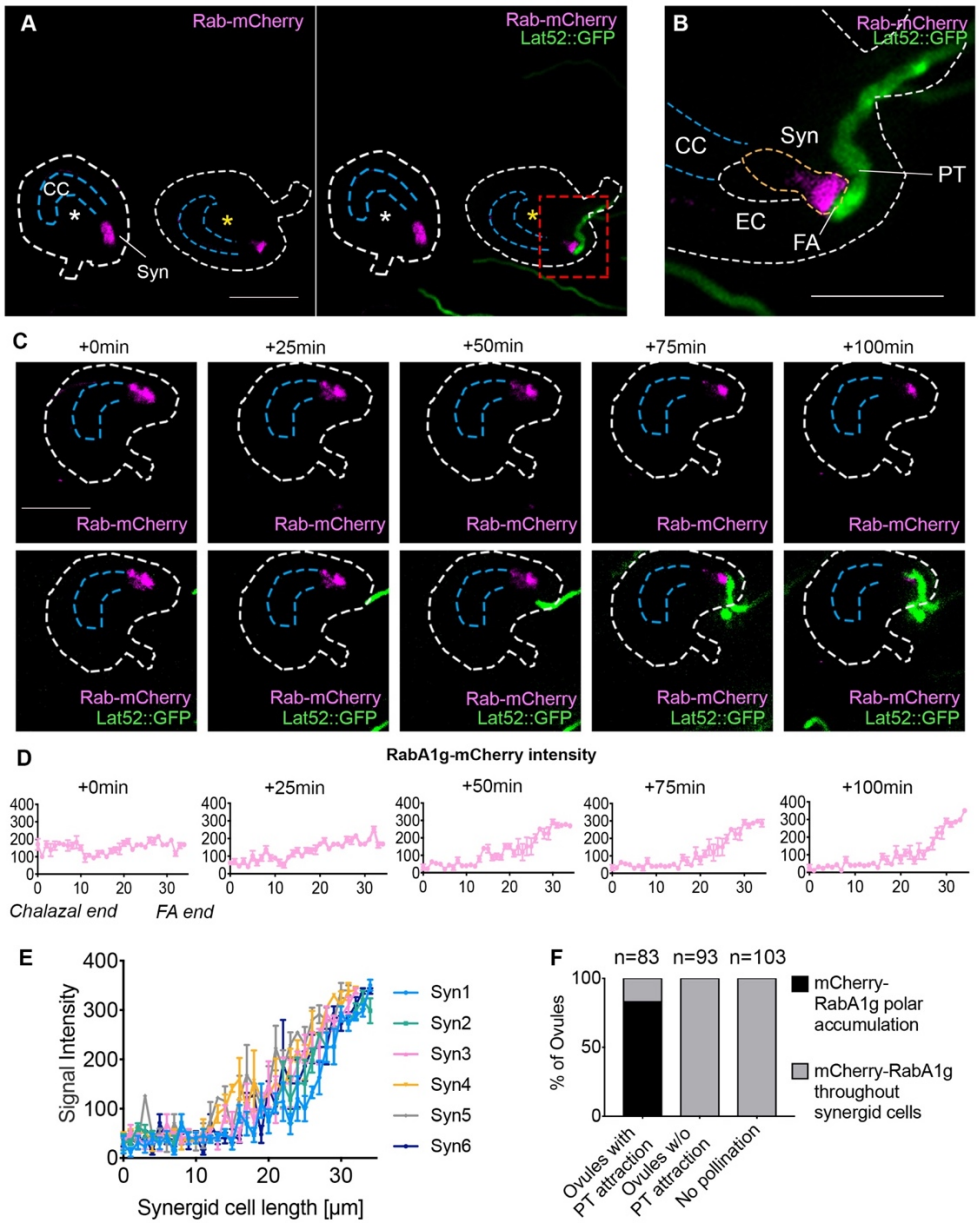

Figure 3. RabA1g endosomes polarly accumulate toward the filiform apparatus during pollen tube reception. (A) RabA1g-mCherry endosome marker (magenta signal) accumulates at the FA region in response to pollen tube arrival (ovule with yellow star). The ovule with no pollen tube attraction (white star) serves as a negative control imaged under the same conditions. (B) Higher magnification of the micropylar region of starred ovule in (red box in panel A). (C) Timing of RabA1g-mCherry polar accumulation during pollen tube arrival. Bars=50µm. (D) Quantification of RabA1g-mCherry signal along the length of synergids during pollen tube reception. Synergid cell from chalazal end to filiform apparatus (FA) end was defined from 0 to 33 µm in length. (E) 6 more examples of the quantification of RabA1g-mCherry signal after pollen tube arrival. (F) Quantification of ovule percentage with RabA1g endosome marker throughout the synergids (gray bars) or with polar accumulation at or near the filiform apparatus (black bars).

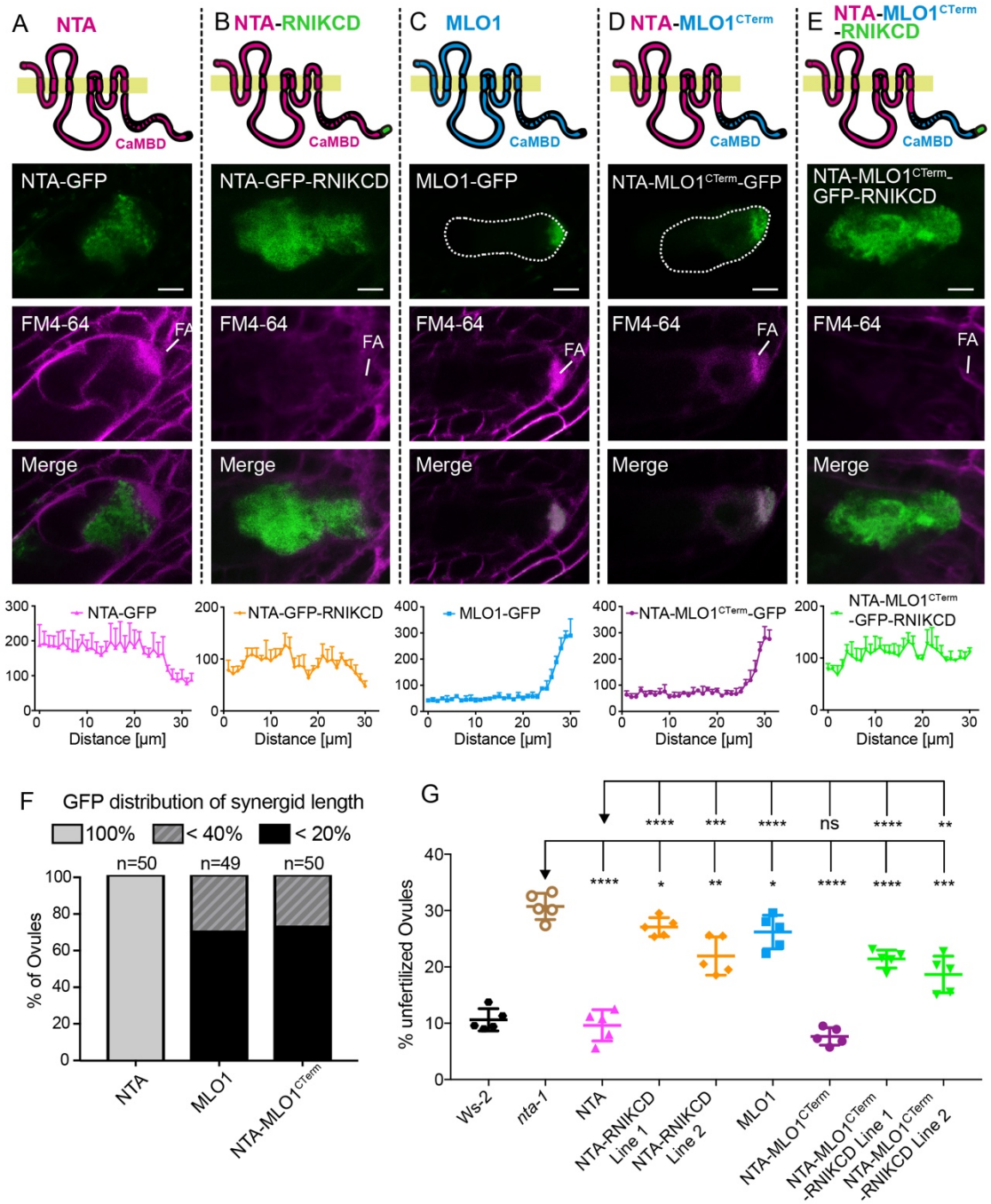

Figure 4. Targeting of NTA to the filiform apparatus before pollen tube arrival is not toxic to synergid cells. (A-E) Localization patterns of MYB98 promoter driven MLO-GFP variants (green signal) in synergids of mature virgin ovules stained with FM4-64 (magenta signal) to reveal the outline of the synergid and the filiform apparatus (FA, diffuse magenta signal). Graphs in each panel show quantification of the GFP intensity of the MLO variants along the length of the synergids. Bars = 10 µm. (F) Percentage of ovules showing MLO-GFP signal throughout the synergids (100% of length), in the FA only (20% of length) and the region surrounding and including the FA (40% of length). (F) Scatter plot of unfertilized ovule percentages in homozygous plants of pMYB98::MLO-GFP in *nta-1* mutants to assess the ability of the MLO-GFP constructs to

complement *nta-1*. WS, Wassilewskija. Significance was determined by a Student's *t*-test (****, $P < 0.0001$; *, $P = 0.0281$; and ns, $P = 0.2020$).

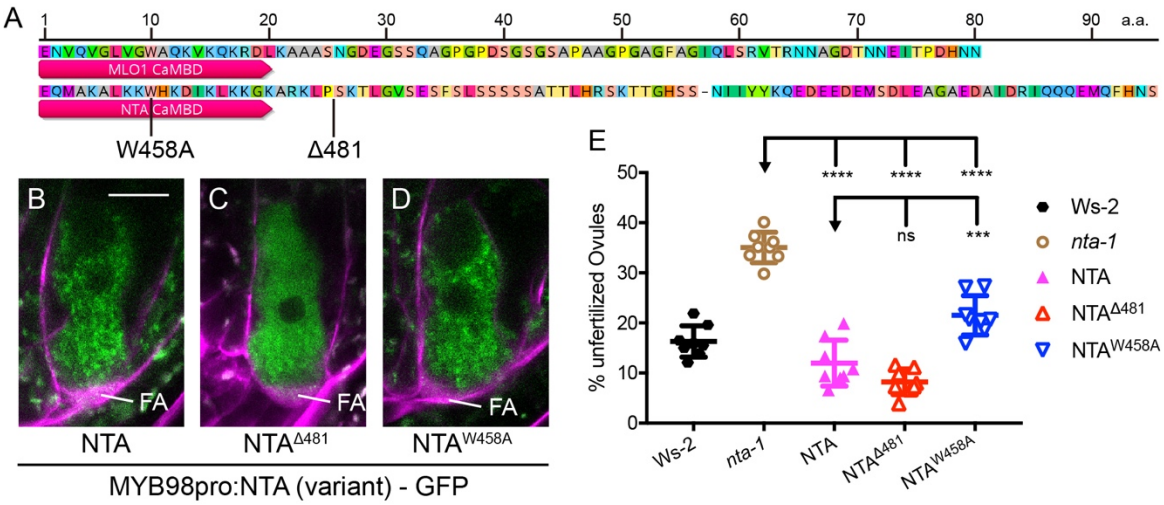

Figure 5. Disruption of the CaMBD affects NTA localization and function. (A) Alignment of MLO1 and NTA C-terminal domains after the seventh membrane span. Red bars highlight the CaMBD; W458A and Δ481 indicate the point mutation in NTA and the deletion point, respectively ; a.a., amino acid. (B-D) NTA (variant)-GFP (green) distribution in synergid cells of unfertilized ovules stained with FM4-64 (magenta signal). Bar = 10 µm. (E) Complementation analysis of NTA variants in T2 plants homozygous for $MYB98_{pro}$::NTA(variant)-GFP constructs in *nta-1* mutants. Adjusted P values from a Student's *t*-test are as follows: **** indicates $P < 0.0001$; *** indicates $P = 0.001$ to 0.0001; and ns indicates $P > 0.05$.

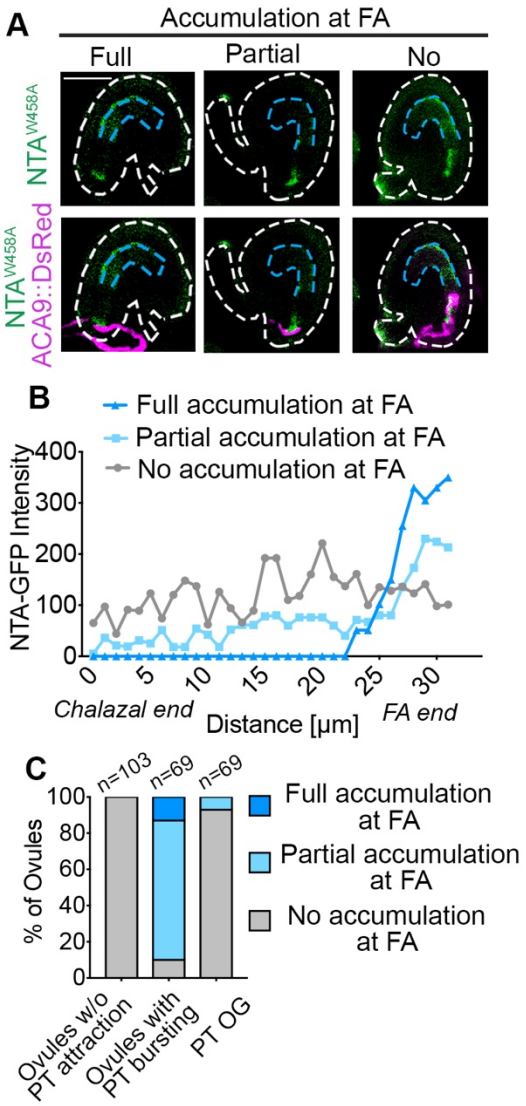

Figure 6. A point mutation in the CaMBD (NTA^{W458A}) affects filiform apparatus accumulation of NTA and pollen tube reception. (A) NTA^{W458A}-GFP has 3 different localization patterns in response to PT arrival under semi *in-vivo* conditions. Bar=50 µm (B) Quantification of GFP signal intensity in NTA^{W458A} synergids during pollen tube reception. (C) Analysis of NTA^{W458A}-GFP distribution patterns in ovules with successful (PT bursting) and unsuccessful (no PT or PT overgrowth (PT OG)) pollen tube reception.

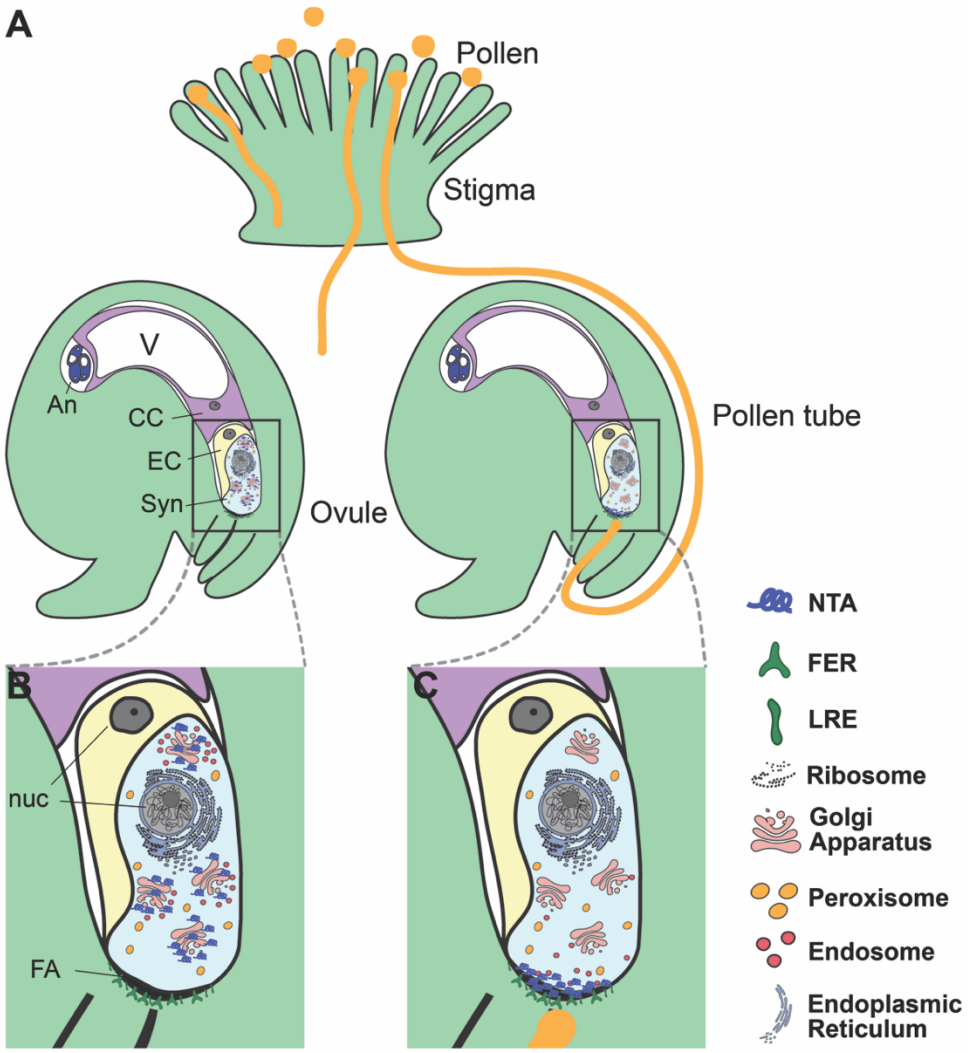

Figure 7. Subcellular dynamics in synergids during pollen tube reception. (A) Pollination using a semi-*in vivo* pollen tube guidance assay. (B) Before pollen tube arrival, NTA is in a Golgi-associated compartment and RabA1g endosomes are distributed throughout the synergids. (C) As a pollen tube arrives, NTA and RabA1g endosomes move toward the filiform apparatus (FA). NTA accumulation is dependent on signaling from the FER receptor like kinase, which acts in a complex with LRE. Abbreviations: CC, Central Cell; Syn, Synergid cells; EC, Egg Cell; An, Antipodal cells; nuc, Nucleus; FA, Filiform Apparatus.

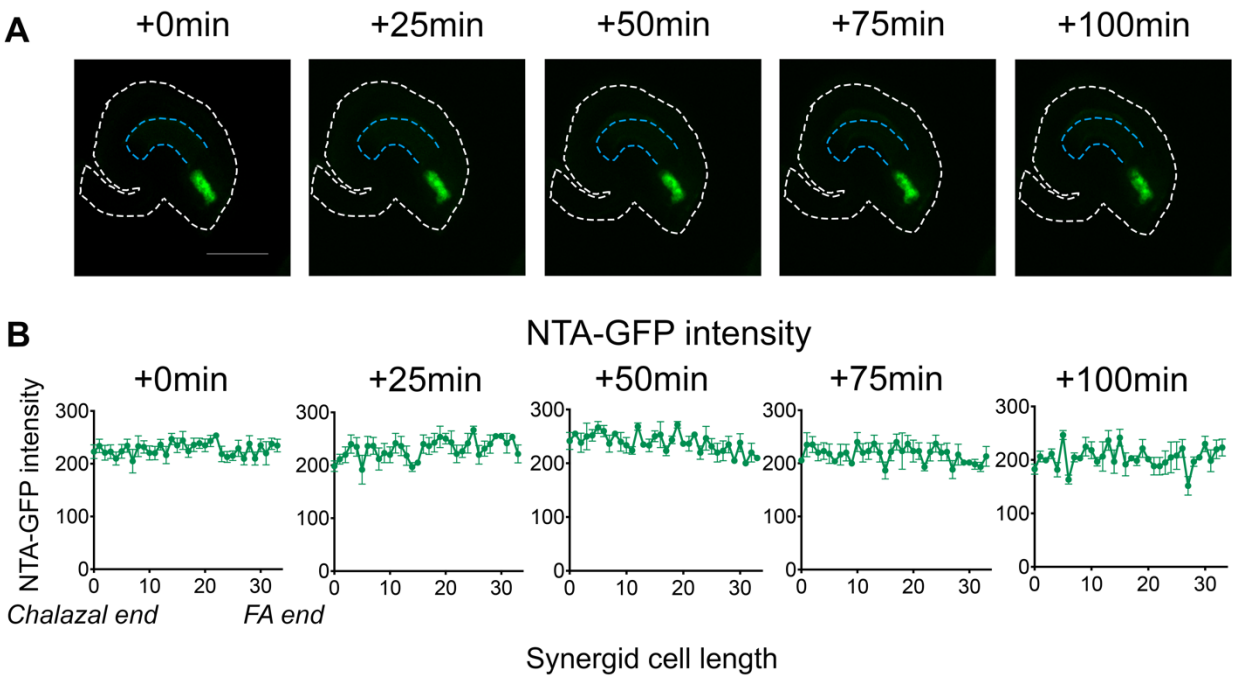

Supplementary figure 1. NTA-GFP does not polarly accumulate at the filiform apparatus in synergids without pollen tube attraction. (A) NTA-GFP (green signal) distribution pattern in synergids at 0min, 25min, 50min, 75min, and 100min timepoints, respectively. (B)Signal intensity measurement of NTA-GFP intensity at 0min, 25min, 50min, 75min, and 100min timepoints, respectively. Bar=50μm.

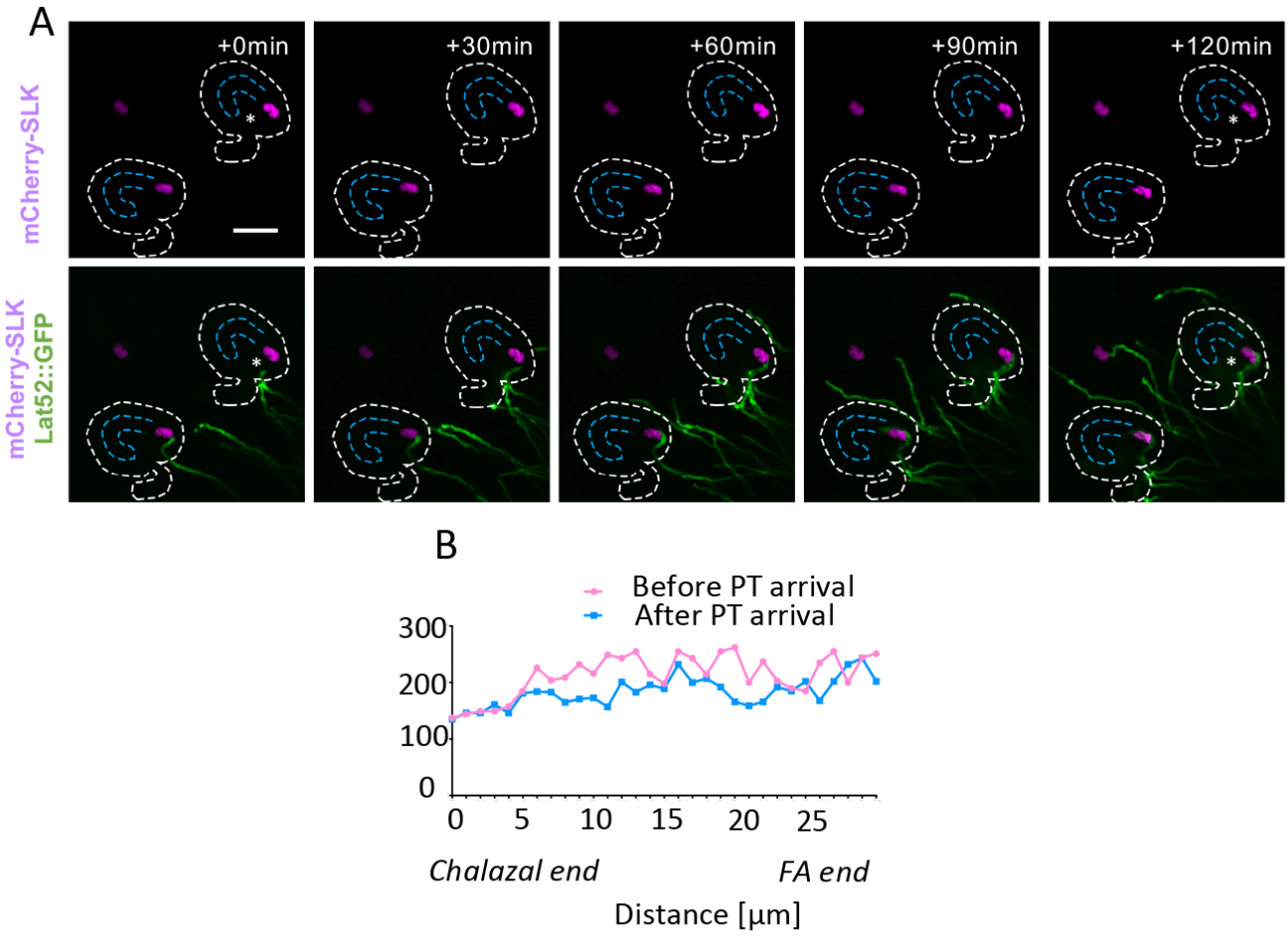

Supplementary figure 2. Peroxisomes do not exhibit polar accumulation at the FA during pollen tube reception. (A) The peroxisome marker mCherry-SLK (magenta signal) does not accumulate to the FA region after pollen tube (green signal) arrival. (B) Quantification of mCherry-SLK signal before and after PT arrival in the ovule with the white star. Bars=50µm.

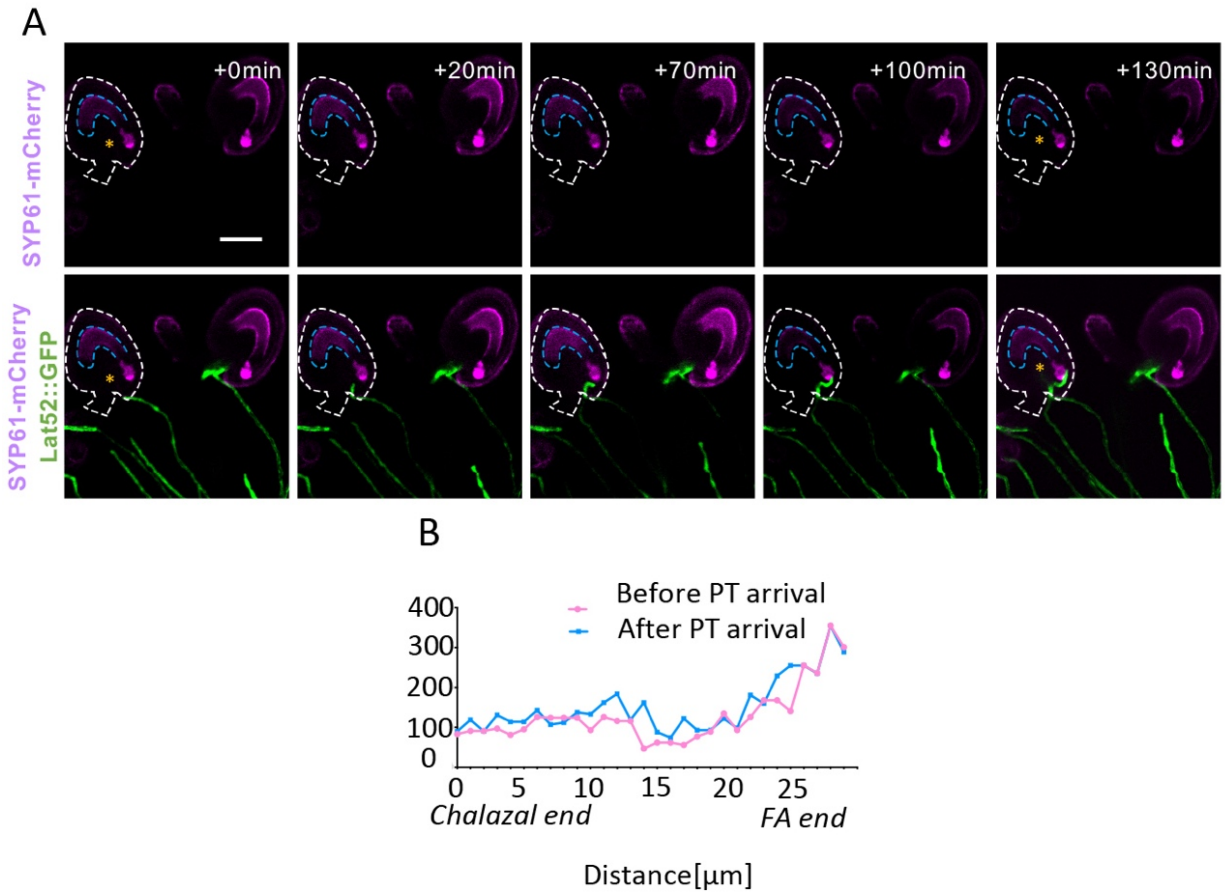

Supplementary figure 3. Trans-Golgi marker distribution in synergids does not change in response to pollen tube reception. (A) The trans-Golgi marker SYP61-mCherry (magenta signal) is concentrated toward the micropyle region of synergid cells both before and after pollen tube (green signal) arrival (ovules with yellow stars). (B) Quantification of SYP61-mCherry signal along the length of a synergid before and after pollen tube reception. Bars=50µm.

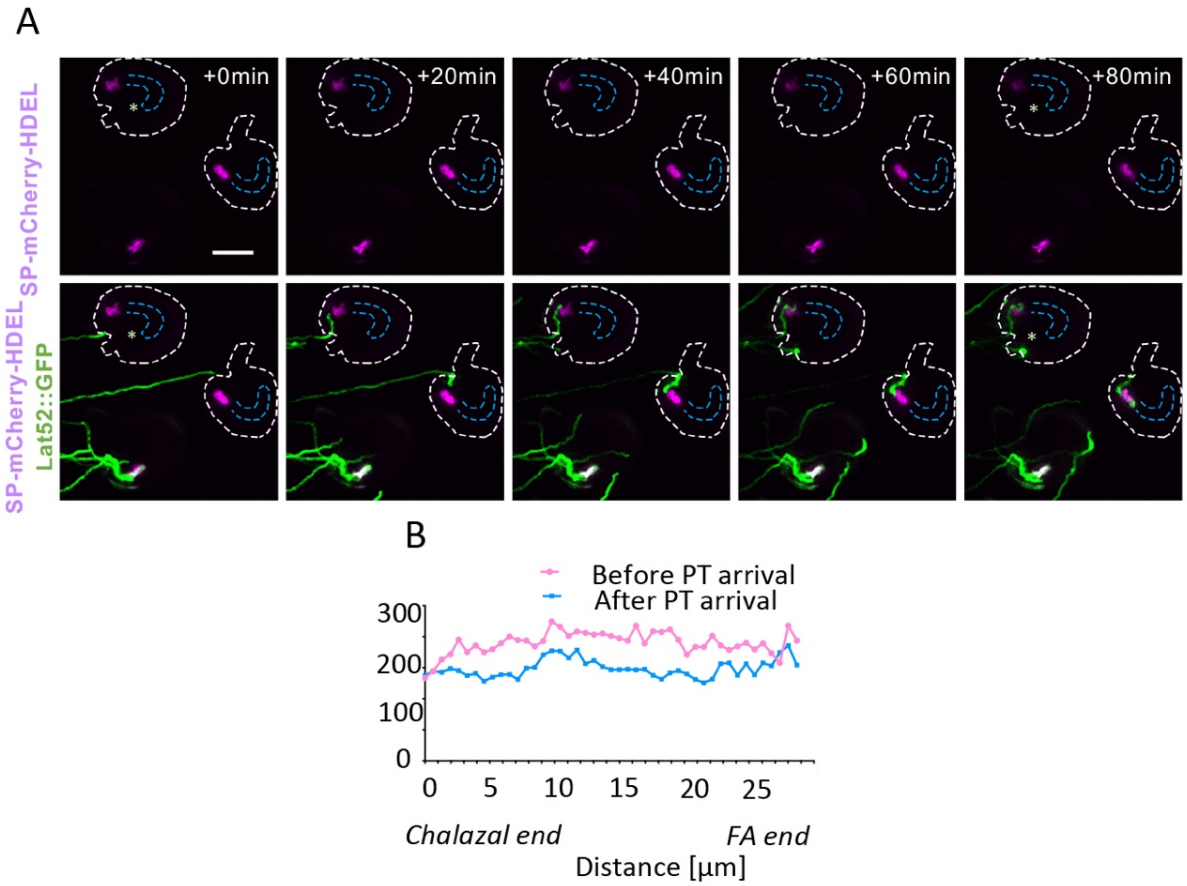

Supplementary figure 4. ER marker distribution in synergids does not change in response to pollen tube reception. (A) Before and after pollen tube (green signal) arrival, the ER marker SP-mCherry-HDEL (magenta signal) is distributed throughout synergid cells. (B) Quantification of SP-mCherry-HDEL signal along the length of synergids in ovule with white star before and after pollen tube reception. Bars=50µm.

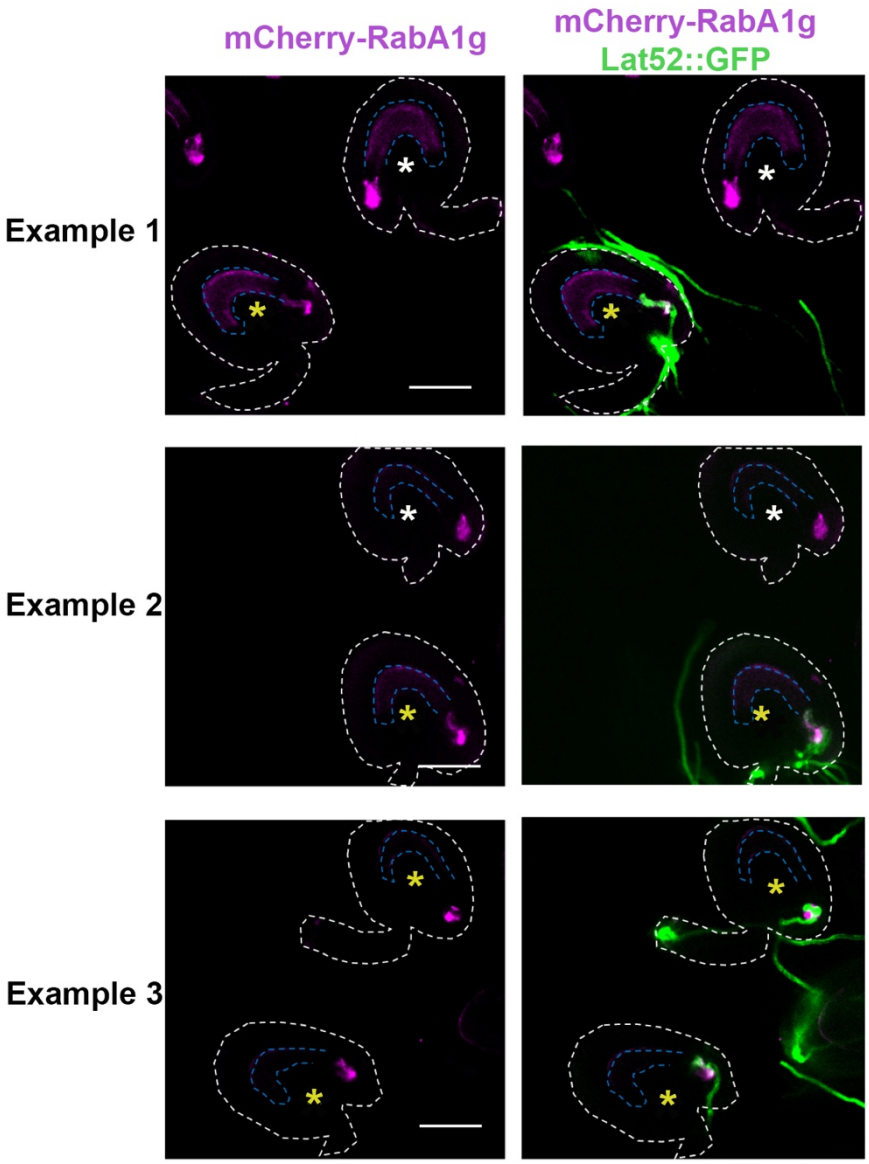

Supplementary figure 5. **Additional examples of the polar accumulation of RabA1g endosomes during pollen tube reception.** Endosome marker accumulates near the filiform apparatus region as pollen tube approaches (ovules with yellow stars), but no polar accumulation was found in ovules that did not attract a pollen tube (ovules with white stars). Bars=50μm.

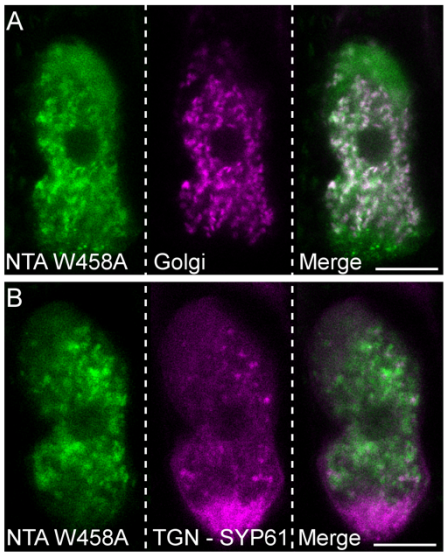

Supplementary figure 6. NTA^{W458A} co-localizes with Golgi marker in synergid cells before pollen tube arrival. Colocalization of NTA^{W458A}-GFP (green) with Golgi marker (*LRE::proMan49-mCherry*, magenta) (A) and the trans-Golgi network marker (TGN, *MYB98pro::SYP61:mCherry*, magenta) (B) in the synergid cell of unpollinated ovules. Bars = 10 μm.

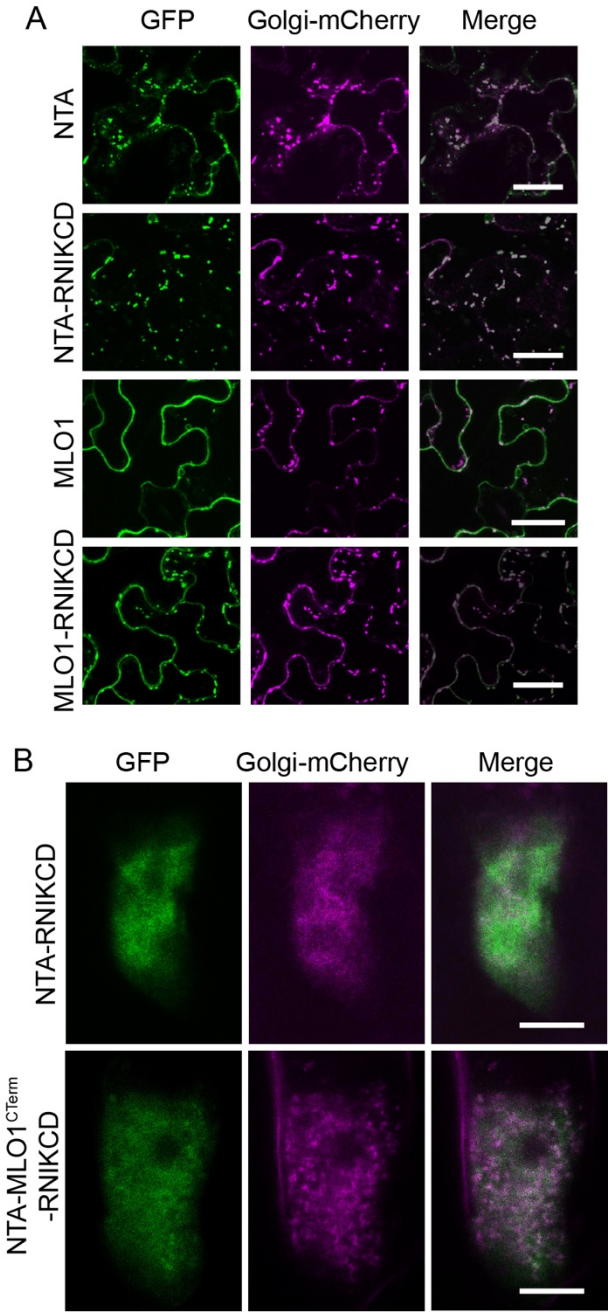

Supplementary figure 7. **A C-terminal Golgi retention signal retains MLO1 and NTA variants in the Golgi.** (A) Colocalization of MLO-GFP (green) with the Golgi-mCherry marker (magenta) indicates that the Golgi retention signal RNIKCD partially retains MLO1 in the Golgi in transiently-transformed tobacco epidermis, Bars = 20 μm. (B) Colocalization of MLO-RNIKCD (green) with the Golgi-mCherry marker (magenta) indicates that the Golgi retention signal RNIKCD retains NTA-MLO1^{CTerm} in the Golgi in the synergid. Bars = 10 μm.

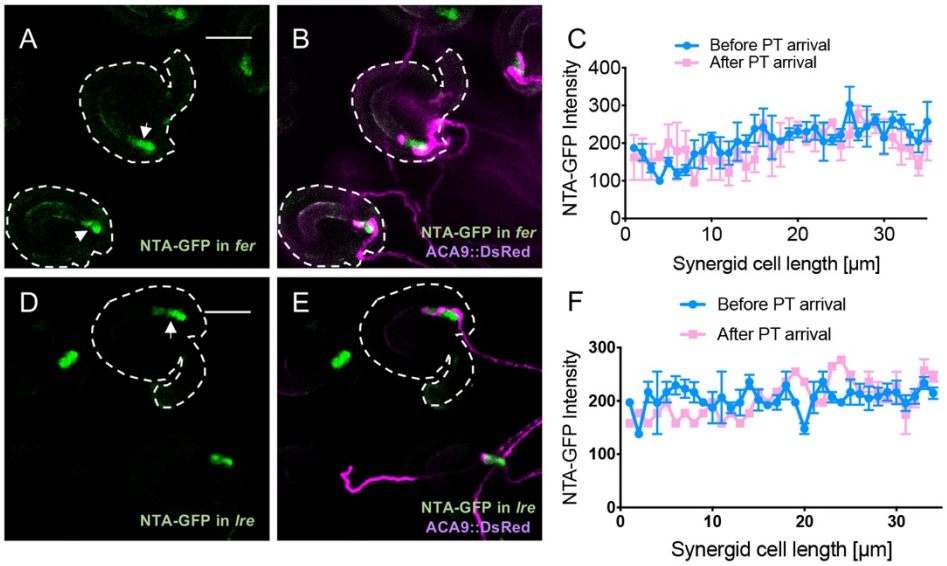

Supplementary figure 8. **NTA-GFP polar accumulation requires FER and LRE.** (A-B) In *fer* mutant synergids, NTA-GFP (green signal) distributes throughout synergids (arrows) with ACA9::DsRed pollen tube overgrowth (magenta signal). (C) Quantification of NTA-GFP signal along the length of *fer-1* synergids before and after pollen tube reception. (D-E) In *lre-7* ovules, NTA-GFP distributes throughout synergids (white arrow) with pollen tube overgrowth. (F) Quantification of NTA-GFP signal along the length of *lre-7* synergids before and after pollen tube reception. FA, Filiform Apparatus. Bars=50µm.

Supplementary table 1. List of primers used for cloning.

Primer Name	Primer Sequences (5' to 3')
NTA-FattB1	GGGGACAAGTTTGTACAAAAAAGCAGGCTTCACCATGATCACAAGAAGCAGGTGT
NTA481-RattB2	GGGGACCACTTTGTACAAGAAAGCTGGGTGTGAAACACCAAGTGTCTTGCT
NTAW458A-R	C**GC**CTTCTTCAATGCCTTTGCCAT
NTAW458A-F	GCATTGAAGAAG**GC**GCACAAAGACATCAAATTGAAGAAAG
NTA-RattB2	GGGGACCACTTTGTACAAGAAAGCTGGGTGAGAGTTGTGGAATTGCATCTC
NTA-R19	CTCATCAAACACTGCTTTCTTCATG
MLO1-F	GCAGTGTTTGATGAGAATGTGCAGGTTGGTCTTGTTG
MLO1-RattB2	GGGGACCACTTTGTACAAGAAAGCTGGGTGGTTGTTATGATCAGGTGTAATCTCA
NTA-Gly5-GFP-R	TTCTCCTTTACTCATTCCTCCTCCTCCACCAGAGTTGTGGAATTG
NTA-Gly5-GFP-F	CAATTCCACAACTCTGGTGGAGGAGGAGGAATGAGTAAAGGAGAA
GFP-RNIKCD-RattB2	GGGGACCACTTTGTACAAGAAAGCTGGGTGCTAGTCGCACTTGATGTTTCTTTTGTATAGTTC
MLO1-Gly5-GFP-R	TTCTCCTTTACTCATTCCTCCTCCTCCACCGTTGTTATGATCAGG
MLO1-Gly5-GFP-F	CCTGATCATAACAACGGTGGAGGAGGAGGAATGAGTAAAGGAGAA

Supplemental Movies

Supplementary movie 1. NTA-GFP (green signal) redistributes to filiform apparatus region as ACA9::DsRed labeled pollen tube (magenta signal) approaches.

Supplementary movie 2. NTA-GFP (green signal) redistributes to filiform apparatus region during pollen tube reception (GFP channel only, same movie as S1).

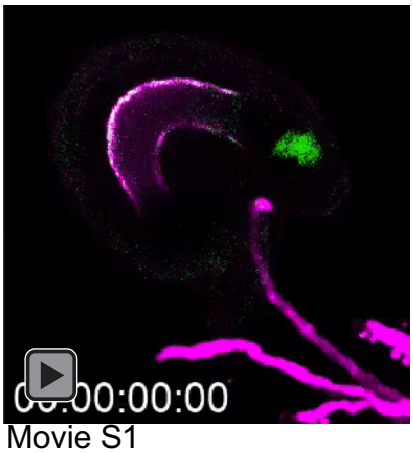

Movie S1

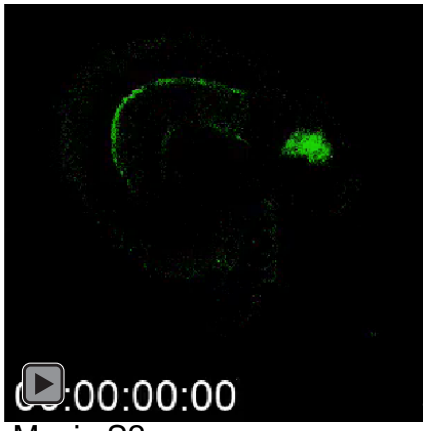

Movie S2

Supplementary movie 3. Golgi-mCherry signals (magenta signal) are evenly distributed along the length of the synergid as Lat52::GFP labeled pollen tube (green signal) approaches.

Supplementary movie 4. Golgi-mCherry signals (magenta signal) are evenly distributed along the length of the synergid during pollen tube reception (mCherry channel only, same movie as S3).

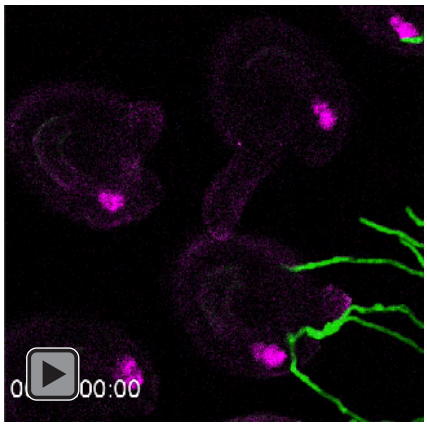

Movie S3

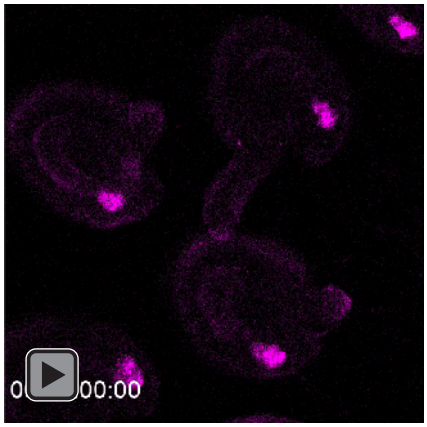

Movie S4

Supplementary movie 5. The trans-Golgi marker SYP61-mCherry (magenta signal) is localized toward the micropyle region of synergid cells both before and after pollen tube (green signal) arrival.

Supplementary movie 6. The trans-Golgi marker SYP61-mCherry (magenta signal) is localized toward the micropyle region of synergid cells during pollen tube reception (mCherry channel only, same movie as S5).

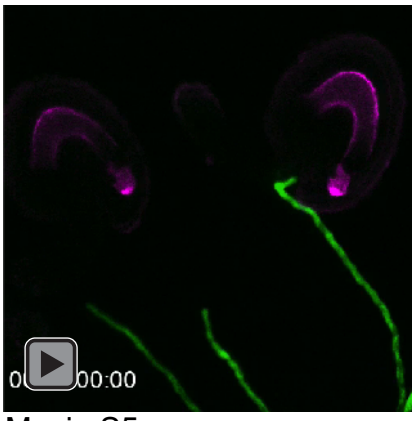

Movie S5

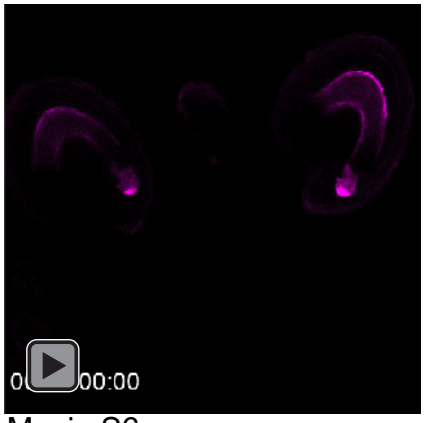

Movie S6

Supplementary movie 7. Before and after pollen tube (green signal) arrival, the ER marker SP-mCherry-HDEL (magenta signal) is distributed throughout synergid cells.

Supplementary movie 8. The ER marker SP-mCherry-HDEL (magenta signal) is distributed throughout synergid cells (mCherry channel only, same movie as S7).

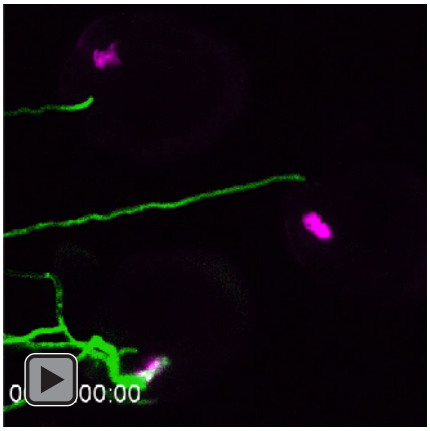

Movie S7

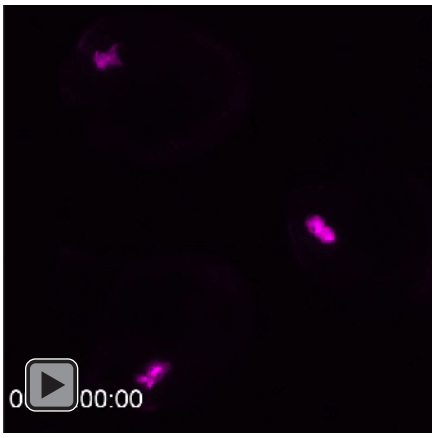

Movie S8

Supplementary movie 9. The peroxisome marker mCherry-SLK (magenta signal) does not redistribute to the filiform apparatus region after pollen tube (green signal) arrival.

Supplementary movie 10. The peroxisome marker mCherry-SLK (magenta signal) does not redistribute to the filiform apparatus region during pollen tube reception (mCherry channel only, same movie as S9).

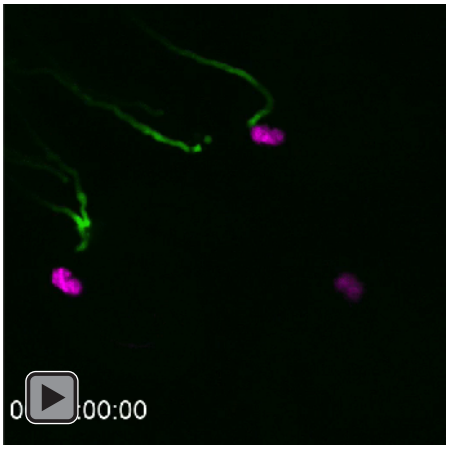

Movie S9

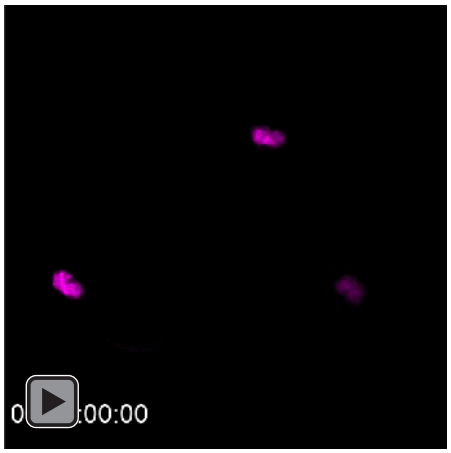

Movie S10

Supplementary movie 11. RabA1g-mCherry endosome marker (magenta signal) accumulates at the filiform apparatus region in response to pollen tube (green signal) arrival.

Supplementary movie 12. RabA1g-mCherry endosome marker (magenta signal) accumulates at the filiform apparatus region during pollen tube reception (mCherry channel only, same movie as S11).

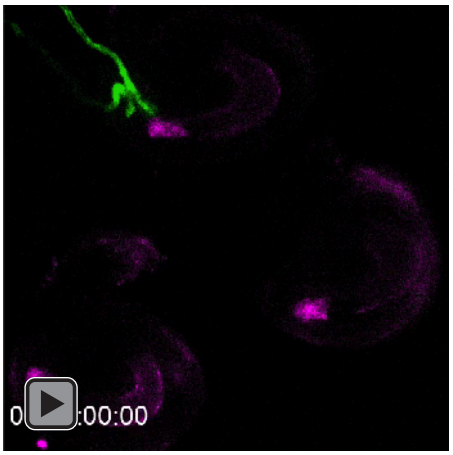

Movie S11

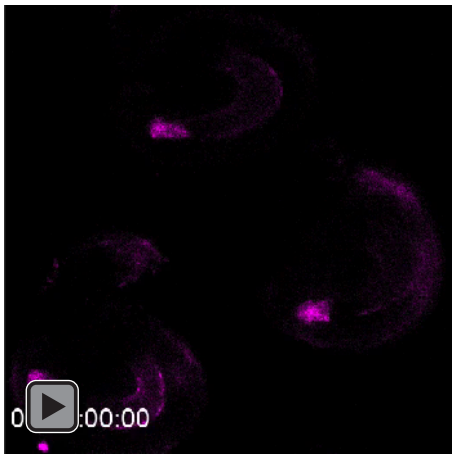

Movie S12